RESOURCE

nature immunology

Programs for the persistence, vigilance and control of human CD8+ lung-resident memory T cells

Pleun Hombrink[1], Christina Helbig[1,7], Ronald A Backer[1,7], Berber Piet[2,7], Anna E Oja[1], Regina Stark[1], Giso Brasser[1], Aldo Jongejan[3], René E Jonkers[4], Benjamin Nota[5], Onur Basak[6], Hans C Clevers[6], Perry D Moerland[3,8], Derk Amsen[1,8] & René A W van Lier[1,8]

Tissue-resident memory T cells (T_{RM} cells) in the airways mediate protection against respiratory infection. We characterized T_{RM} cells expressing integrin α_E (CD103) that reside within the epithelial barrier of human lungs. These cells had specialized profiles of chemokine receptors and adhesion molecules, consistent with their unique localization. Lung T_{RM} cells were poised for rapid responsiveness by constitutive expression of deployment-ready mRNA encoding effector molecules, but they also expressed many inhibitory regulators, suggestive of programmed restraint. A distinct set of transcription factors was active in CD103+ T_{RM} cells, including Notch. Genetic and pharmacological experiments with mice revealed that Notch activity was required for the maintenance of CD103+ T_{RM} cells. We have thus identified specialized programs underlying the residence, persistence, vigilance and tight control of human lung T_{RM} cells.

Viral infections of the airways are a major cause of morbidity and mortality. Since CD8+ T cells are central in host defense against such viral infections[1,2], the ability to generate and maintain effective CD8+ T cell memory is a key objective for vaccine development, with potentially major effects on global health.

Memory CD8+ T cells have traditionally been categorized as central memory T cells (T_{CM} cells) and effector memory T cells (T_{EM} cells). These populations both recirculate in blood and tissues but differ in tissue distribution, immediate effector ability and ability to expand during secondary infection[3]. Published findings have shown that a subset of memory CD8+ T cells does not recirculate but is maintained at the site of infection[4]. These tissue-resident memory T cells (T_{RM} cells) are required for optimal protection at mucosal sites such as the lungs, intestine and female reproductive tract[5,6]. The best-characterized T_{RM} cells express the integrin α_E (CD103) and the C-type lectin CD69, which promote localization to epithelia through interaction with E-cadherin[5] and prevent homing to blood and lymph by interfering with activity of the receptor for the bioactive lipid S1P, respectively[7]. However, published results indicate that some T_{RM} cells express neither CD69 nor CD103 but nonetheless exhibit T_{RM} cell characteristics[8–10]. T_{RM} cells keep recall infections from spreading into the lower airways and thereby curb the development of pathology[1]. This function requires swift responsiveness of these cells. One mechanism used by T_{RM} cells is the production of interferon-γ (IFN-γ), which promotes antiviral resistance of the tissue and induces the production of chemokines to recruit auxiliary immune cells[11]. Remaining in tissues after clearance of infection, T_{RM} cells do not have access to the niches in secondary lymphoid organs where circulating memory T cells receive their maintenance signals. How T_{RM} cells are maintained *in situ* is not clear, although signaling via the receptor for interleukin 15 (IL-15) is apparently important[8].

T_{RM} cells in the lungs confer superior protective immunity relative to that provided by circulating T cells[12–14]. Vaccination strategies should therefore aim at eliciting stable antigen-specific T_{RM} cell populations. The ability to design such strategies requires thorough understanding of these cells. Lung T_{RM} cells have been characterized in mouse models[8]. However, it is not clear to what degree such data can be extrapolated to human T cells, given the considerable divergence between these species in genes encoding products associated with immunity[15] and the differences in the time frame associated with immunological memory, spanning decades in humans, compared with a few years in mice[16].

Here we analyzed the genetic programs of memory CD8+ T cell populations obtained from human lung-resection tissues. These populations had gene-expression signatures very different from those of blood-derived T cells. Lung T_{RM} cells constitutively expressed deployment-ready mRNAs encoding effector molecules but also expressed many inhibitory regulators. These cells therefore seemed to be poised for prompt reactivity to pathogens but under tight control to limit impairment of the air-exchange function in the delicate lung mucosa. Furthermore, T_{RM} cells exhibited an active Notch signaling signature, and activity of this pathway was required for their maintenance.

[1]Department of Hematopoiesis, Sanquin Research and Landsteiner Laboratory, Amsterdam, the Netherlands. [2]Department of Experimental Immunology, Academic Medical Center, Amsterdam, the Netherlands. [3]Department of Clinical Epidemiology, Biostatistics and Bioinformatics, Academic Medical Center, Amsterdam, the Netherlands. [4]Department of Respiratory Medicine, Academic Medical Center, Amsterdam, the Netherlands. [5]Department of Blood Cell Research, Sanquin Research and Landsteiner Laboratory, Amsterdam, the Netherlands. [6]Hubrecht Institute-KNAW (Royal Netherlands Academy of Arts and Sciences), Utrecht, the Netherlands. [7]These authors contributed equally to this work. [8]These authors jointly directed this work. Correspondence should be addressed to D.A. (d.amsen@sanquin.nl).

Received 9 June; accepted 21 September; published online 24 October 2016; corrected after print 28 November 2016; doi:10.1038/ni.3589

RESULTS

Distinct transcriptional profile of lung T_{RM} cells

To study lung-resident memory CD8$^+$ T cells, we isolated CD45RA$^-$ T cells from paired samples of healthy lung tissue and peripheral blood from patients undergoing lung resection (**Supplementary Fig. 1**). Many memory CD8$^+$ T cells from the lungs and some from the blood expressed CD103 (**Fig. 1a,b**). Whereas the latter nearly all coexpressed the costimulatory receptor CD27 (**Fig. 1c**) and thus resembled T_{CM} cells, expression of CD27 was low or negative on both CD103$^+$ memory T cells and CD103$^-$ memory T cells from lungs, characteristic of T_{EM} cells (**Fig. 1c**). The CD103$^+$ population from lungs almost universally expressed CD69, but 5–30% of the lung CD103$^-$ population lacked expression of this marker (**Fig. 1d**).

We determined by microarray the global gene-expression profiles of CD103$^+$ and CD103$^-$ memory CD8$^+$ T cell subsets from the lungs and blood by isolating mRNA directly *ex vivo* and after stimulation of cells with antibody to the invariant signaling protein CD3 (anti-CD3) and antibody to the co-receptor CD28 (anti-CD28). CD103$^-$ memory T cells from blood were additionally selected for lack of CD27 expression to obtain T_{EM} cells (populations that included >95% CCR7$^-$ cells; **Supplementary Fig. 1**). The results of this microarray analysis were confirmed by quantitative PCR analysis of ten genes (**Supplementary Fig. 2**).

We used lung tissue from two types of patients: non-cancerous lobectomy tissue from patients with non-small cell lung carcinoma, and lung tissue from patients with chronic obstructive pulmonary disease (whose lungs were removed in preparation for lung transplantation). The results of samples from both sources were very similar (**Supplementary Fig. 3**). Principal-component analysis and hierarchical clustering revealed that the expression profiles of unstimulated cells segregated according to anatomical origin rather than by donor or donor type (**Fig. 1e,f**). CD103$^+$ T cells from blood proved more similar to blood-derived CD103$^-$ T_{EM} cells than to the CD103$^+$ subset from lungs (**Fig. 1e,f**), which suggested that most blood-derived CD103$^+$ T cells were not lung T_{RM} cells that had mobilized into circulation. Also, the CD103$^-$ subset from lungs was more similar to the CD103$^+$ lung subset than to either population from the blood (**Fig. 1e,f**). We therefore considered this CD103$^-$ CD8$^+$ memory T cell population from lungs to be mostly tissue resident. We call the CD103$^+$ lung population and CD103$^-$ lung population specifically 'T_{RM}^{103+} cells' and 'T_{RM}^{103-} cells', respectively, here.

Given that blood T_{EM} cells have been well characterized, we used their transcriptome as reference to which we compared the other transcriptomes. The greatest number of differentially expressed genes (897) appeared in the comparison between lung T_{RM}^{103+} cells and blood T_{EM} cells (**Fig. 1g**). Of those, 301 were shared with the lung T_{RM}^{103-} cell subset, while 596 were not (**Fig. 1g**). However, most of those 596 genes also did exhibit a similar expression pattern in the comparison between T_{RM}^{103-} cells and circulating T_{EM} cells (**Supplementary Fig. 4**), but this result did not reach statistical significance. Only 10 genes showed significantly differential expression in the lung memory CD8$^+$ T cell populations (**Supplementary Fig. 4**). Likewise, only a limited number of genes (50) had differential expression in the two blood-derived populations

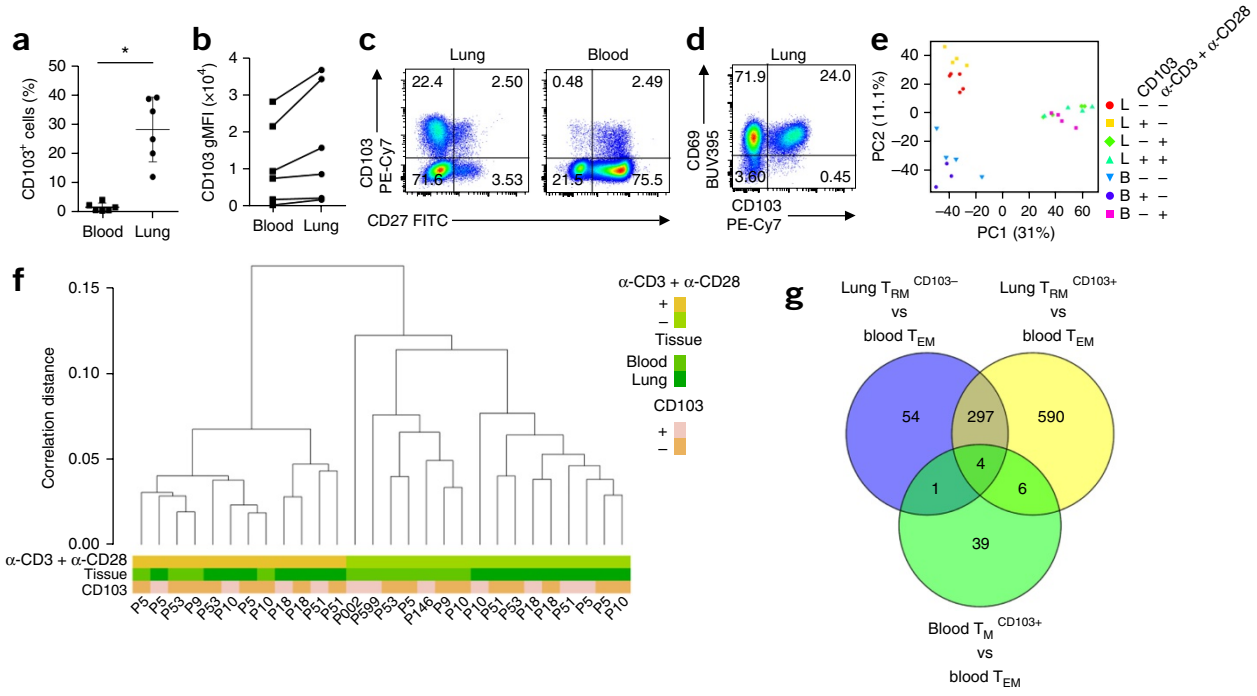

Figure 1 Distinct gene-expression program of lung T_{RM} cells. (**a**) Frequency of CD103-expressing memory CD8$^+$ T cells in paired samples ($n = 6$) from the peripheral blood and lungs (horizontal axis), measured by flow cytometry. Each symbol represents an individual donor; small horizontal lines indicate the mean (± s.d.). (**b**) Geometric mean fluorescence intensity (gMFI) of CD103 on paired sets of CD103$^+$CD8$^+$ T cells derived from the peripheral blood and lungs (lines connect paired samples). (**c**) Flow cytometry (bi-exponential scales) analyzing the expression of CD103 and CD27 on CD8$^+$ T cells derived from the lungs (left) and blood (right). Numbers in quadrants indicate percent cells in each throughout. (**d**) Flow cytometry analyzing the expression of CD69 and CD103 on lung-derived CD8$^+$ T cells. (**e**) Principal-component analysis of global gene-expression data for CD8$^+$ memory T cell subsets derived from the lungs (L) or blood (B) ($n = 6$ donors) that expressed CD103 (+) or not (–), assessed under resting conditions (–) or after stimulation (+) for 16 h with anti-CD3 plus anti-CD28 (α-CD3 + α-CD28) (key). Each symbol represents a cell population from an individual donor; PC1 and PC2 indicate principal components 1 and 2. (**f**) Hierarchical clustering of T cell populations as in **e** (key; horizontal axis); bottom ('P' and number), donor identification. (**g**) Quantification of genes with significantly differential expression in various comparisons (periphery) of T cell subsets (with a false-discovery rate (FDR) of <0.05), and overlap among those groups. *$P < 0.001$ (paired *t*-test). Data are representative of three experiments (**a**,**b**), nine independent experiments (**c**,**d**) or one experiment (**e**–**g**).

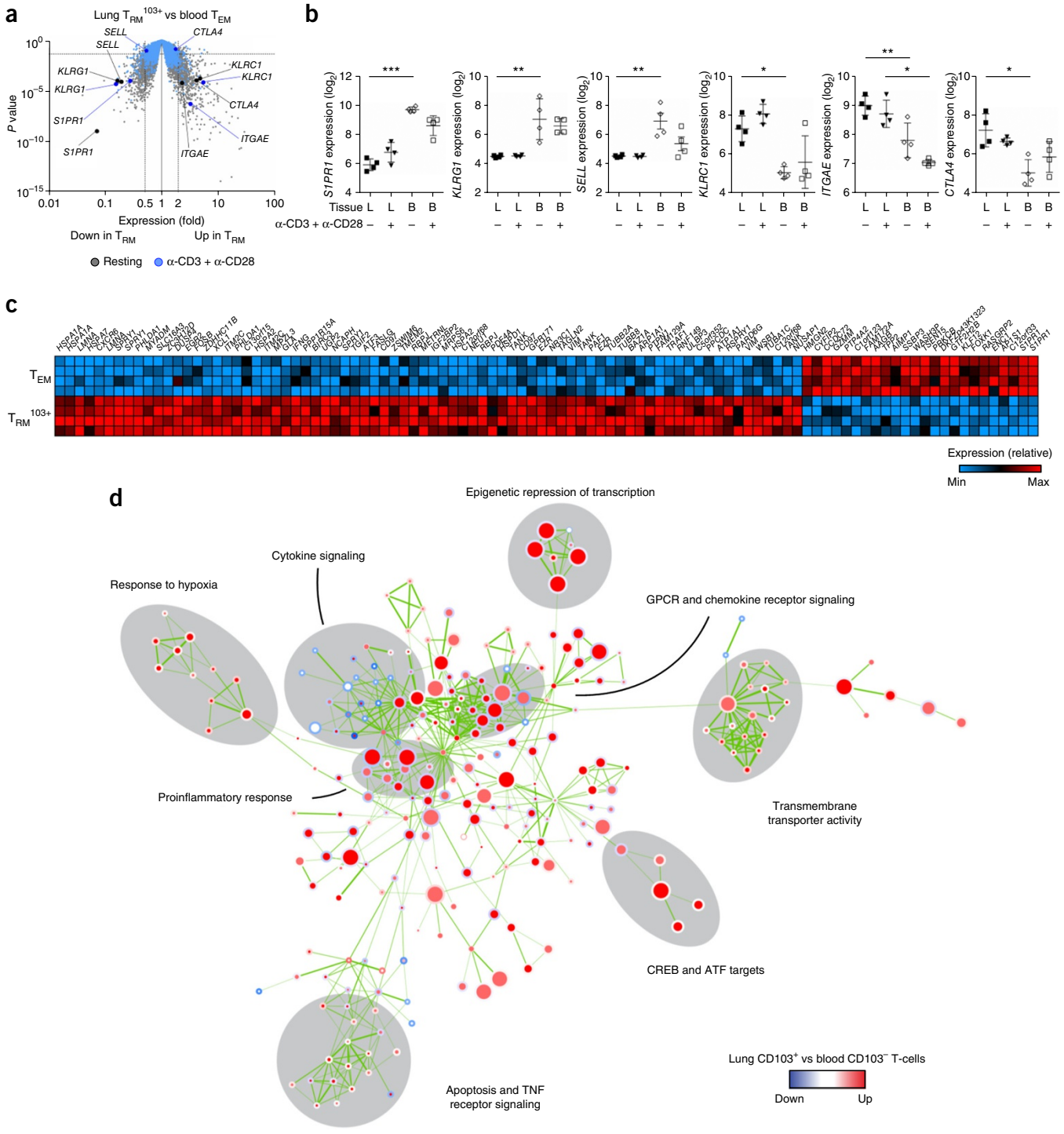

Figure 2 Top differentially expressed genes and gene sets in lung T_{RM} cells. (**a**) Gene expression in lung T_{RM}^{103+} cells versus that in peripheral-blood-derived T_{EM} cells under resting conditions or after stimulation with anti-CD3 plus anti-CD28 (key), showing genes upregulated (Up in T_{RM}; right) or downregulated (Down in T_{RM}; left) in the T_{RM}^{103+} cells relative to their expression in the T_{EM} cells (dashed vertical lines indicate a 0.5-fold or 2-fold difference in expression or no difference (1-fold) in expression), plotted against *P* values (dashed horizontal line indicates $P = 0.05$). Each symbol represents an individual probe set (key T_{RM} cell genes are labeled). (**b**) Expression (log_2-transformed normalized values) of various genes (vertical axes) in T cell subsets derived from the lungs or blood and analyzed under resting conditions or after stimulation with anti-CD3 plus anti-CD28 (below plots). *FDR < 0.05, **FDR < 0.01 and ***FDR < 0.001. Each symbol represents an individual donor; small horizontal lines indicate the mean (± s.d.). (**c**) Expression of mRNA from the top 100 genes (above plot) with the greatest difference in expression (key) in lung T_{RM}^{103+} cells relative to that in blood T_{EM} cells (left margin), under resting conditions. (**d**) Gene-set–enrichment analysis of lung T_{RM}^{103+} cells versus blood T_{EM} cells: labels along periphery indicate prominent biological functional categories (grouped by gray ellipses); nodes represent gene sets (derived from the Molecular Signatures Database (MSigDB)) with differential expression in lung T_{RM}^{103+} cells relative to that in blood-derived T_{EM} cells; node color and intensity indicate degree of significance of enrichment, and node size is proportional to the number of genes in the set; circles represent comparison between resting samples (inner circles) or stimulated samples (outer circles). Data are representative of one experiment.

Table 1 Enriched gene sets

Gene-set name	MSigDB 5.1 or PMID	Genes in set	Direction	FDR
Genes upregulated in T cells by glucose deprivation	PMID: 26321681	9	Up	0.012
Induction of apoptosis through death-receptor signaling	GSEA: M14971	28	Up	0.017
Atpase activity coupled to transmembrane movement of ions	GSEA: M10590	15	Up	0.017
Genes involved in peptide-ligand-binding receptors	GSEA: M12289	110	Up	0.038
Genes upregulated by IFN-γ and TNF activation	PMID: 21093321	147	Up	0.038
Genes suppressed by histone deacetylases HDAC1 and HDAC2	GSEA: M18938	195	Up	0.043
$CD4^+$ T cells treated with TGF-β and IL-4	GSEA: M6075	162	Up	0.048
Protein kinase AKT signaling	GSEA: M15258	17	Up	0.048
Genes encoding the NF-κB core signaling proteins	GSEA: M8804	11	Up	0.048
Genes involved in chemokine receptor signaling	GSEA: M625	44	Up	0.049

Ten prominent gene sets enriched (CAMERA analysis) in lung T_{RM} cells versus blood T_{EM} cells under resting conditions. MSigDB 5.1, Molecular Signatures Database version 5.1; PMID, PubMed identifier; GSEA, gene-set–enrichment analysis.

(**Fig. 1g**). We concluded that both lung-derived T cell subsets were distinct from blood memory $CD8^+$ T cells and were related (but not identical) to each other. Because T_{RM}^{103+} cells are the population that dwells in the epithelial barrier and are therefore most acutely involved in maintaining border integrity, we focused further analysis on this subset.

Top differentially expressed genes and gene sets

Comparison of the gene-expression patterns of lung T_{RM}^{103+} cells with those of blood T_{EM} cells yielded genes encoding the factors also observed in studies of mice[8,17]. Expression of *ITGAE* (which encodes CD103), *CTLA4* (which encodes the immunomodulatory receptor CTLA-4) and *KLRC1* (which encodes the inhibitory receptor NKG2A) was elevated in T_{RM}^{103+} cells, whereas the expression of *S1PR1* (which encodes the S1P receptor), *SELL* (which encodes the lymph-node-homing receptor CD62L) and *KLRG1* (which encodes the activation marker KLRG1) was low (**Fig. 2a**,**b**). Among the top 100 genes with the greatest difference in expression in T_{RM}^{103+} cells relative to that in blood T_{EM} cells were those encoding heat-shock proteins (*HSPA1A*, *HSPA7*, *HSPA2* and *HSPD1*), transcription factors (*EGR2*, *FOSB*, *ATF3* and *RBPJ*), a chemokine (*XCL1*), a chemokine receptor (*CXCR6*), the ligand for the death receptor Fas (*FASLG*), anti-apoptotic factors (*PHLDA1* and *BIRC3*), members of the tumor-necrosis factor (TNF) receptor signaling family (*TRAF1* and *TANK*), an adhesion G-protein-coupled receptor (*CD97*) and interferon-γ (*IFNG*), all of which exhibited higher expression in T_{RM}^{103+} cells than in blood T_{EM} cells (**Fig. 2c**). Furthermore, T_{RM}^{103+} cells 'preferentially' expressed several splice variants of sprouty 1 (encoded by *SPRY1*), which is an inhibitor of signaling via the T cell antigen receptor (TCR)[18] (**Fig. 2c** and **Supplementary Fig. 5**). Genes with much lower expression in T_{RM}^{103+} cells than in blood T_{EM} cells included those encoding the transcription factor Kruppel-like factor 12 (*KLF12*) and granzyme M (*GZMM*) (**Fig. 2c**).

Gene-set–enrichment analysis with the CAMERA gene-set test procedure[19] showed that major differences between T_{RM}^{103+} cells and blood-derived T_{EM} cells were associated with cytokine signaling, chemokine receptor signaling, active transport of ions and small molecules, apoptosis, TNF receptor signaling and the proinflammatory immune response (**Fig. 2d** and **Supplementary Table 1**).

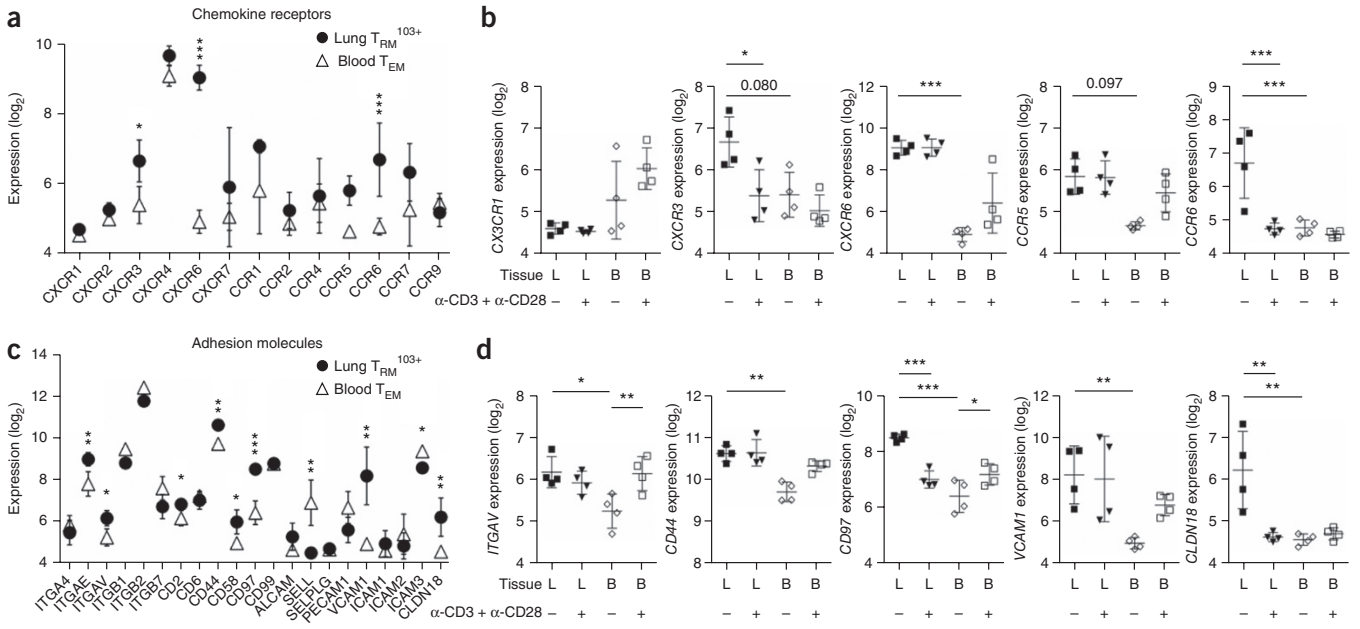

Figure 3 Specific localization program of lung T_{RM}^{103+} cells. (**a**,**c**) Expression (log_2-transformed normalized values) of genes (horizontal axes) encoding chemokine receptors (**a**) or adhesion molecules (**c**) in lung T_{RM}^{103+} cells and blood T_{EM} cells (keys) under resting conditions. (**b**,**d**) Expression (as in **a**) of genes (vertical axes) encoding chemokine receptors (**b**) or adhesion molecules (**d**) in lung- or blood-derived T cell subsets under resting conditions or after stimulation with anti-CD3 plus anti-CD28 (below plots). *FDR < 0.05, **FDR < 0.01 and ***FDR < 0.001 (other FDR values above bracketed comparisons). Each symbol represents an individual donor; small horizontal lines indicate the mean (± s.d.). Data are representative of one experiment.

The gene set most highly enriched among the genes with differential expression between these two cell types indicated that T_{RM}^{103+} cells exhibited a glucose-deprivation signature (**Table 1**), consistent with the lower glucose concentration in airway fluid than in blood[20]. Gene sets encoding products related to hypoxia were also enriched in this comparison (**Fig. 2d** and **Supplementary Table 1**). Correspondingly, lung T_{RM}^{103+} cells had elevated expression of *HIF1A* mRNA (which encodes HIF-1α) and *EPAS1* mRNA (which encodes HIF-2α) (**Supplementary Fig. 5**).

Chemokine and homing receptors

The distinct anatomical localization of lung T_{RM}^{103+} cells required specific migratory properties, as reflected by enrichment for gene sets encoding chemokine receptors, among the genes with differential expression in lung T_{RM}^{103+} cells relative to that in blood-derived T_{EM} cells (**Fig. 2d**). Receptors that distinguished lung T_{RM}^{103+} cells from circulating T_{EM} cells included CXCR3, CXCR6, CCR5 and CCR6 (**Fig. 3a**,**b**). With the exception of CCR6, which could not be reliably detected anymore after collagenase treatment, elevated expression of these receptors was confirmed by flow cytometry (**Supplementary Fig. 6**). Of these, CCR6 also had high expression in $CD103^+$ memory $CD8^+$ T cells from the blood (**Supplementary Fig. 5b**) and was therefore not sufficient for localization to the lung epithelium. Furthermore, T_{RM}^{103+} cells expressed little CX3CR1 (**Fig. 3b**), a chemokine receptor that mediates transmigration through endothelial layers[21]. Low expression of this receptor in T_{RM}^{103+} cells fits with the hypothesis that these cells had reached their target destination and did not need to interact with endothelium.

The repertoire of adhesion molecules in lung T_{RM}^{103+} cells was also different from that in blood T_{EM} cells. Apart from their high expression

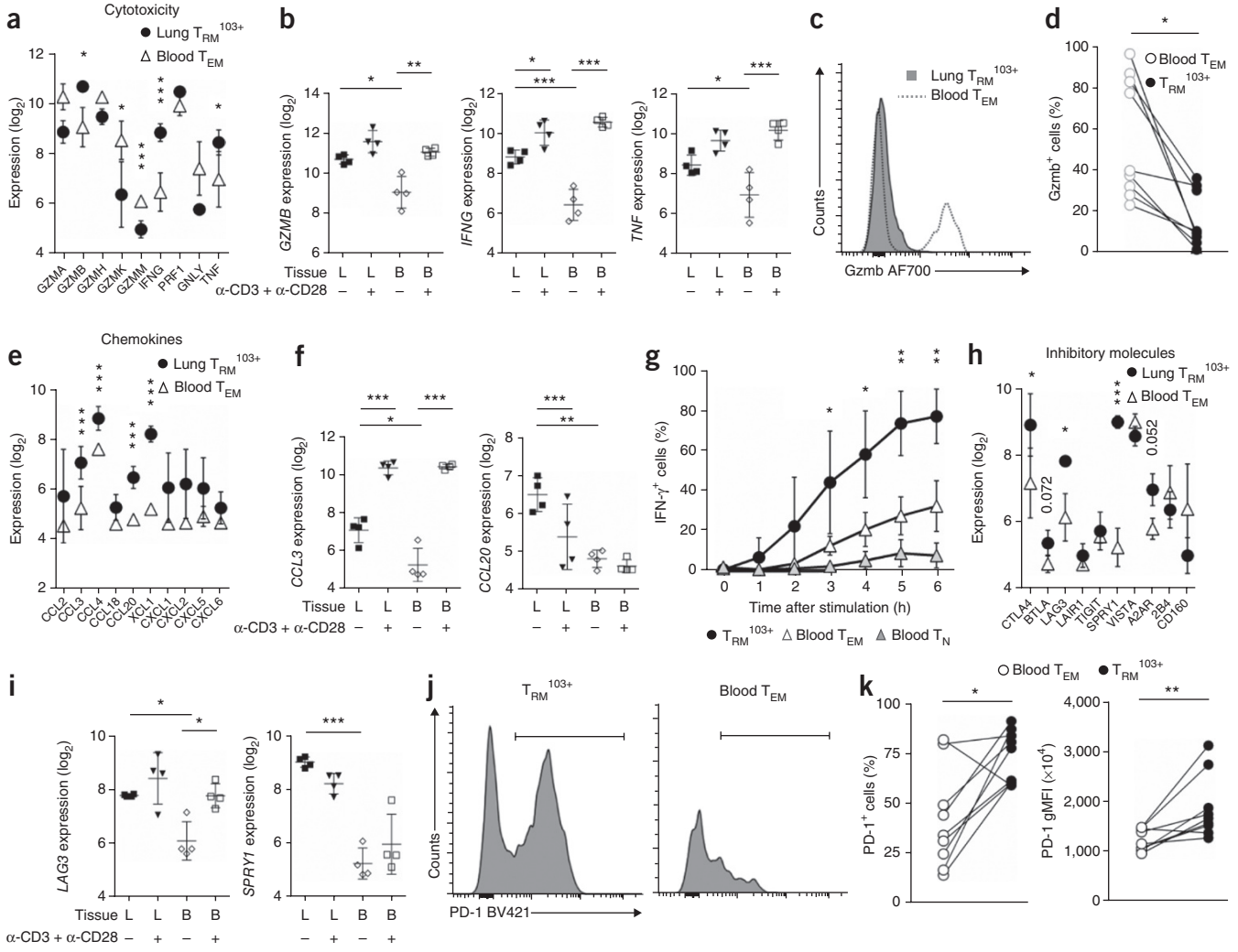

Figure 4 Rapid but strictly regulated effector function of lung T_{RM}^{103+} cells. (**a**,**e**,**h**) Expression (log_2-transformed normalized values) of genes (horizontal axes) encoding cytotoxic mediators (**a**), chemokines (**e**) or inhibitory molecules (**h**) in lung and blood T cell subsets (key) under resting conditions. (**b**,**f**,**i**) Expression (as in **a**) of various genes (horizontal axes) in lung- and blood-derived T cell subsets under resting conditions or after stimulation with anti-CD3 plus anti-CD28 (below plots). (**c**,**d**) Flow cytometry (**c**) and quantification (**d**) of granzyme B (Gzmb) in paired samples ($n = 9$) of lung T_{RM}^{103+} cells and blood T_{EM} cells (keys); lines (**d**) connect paired samples. (**g**) Frequency of IFN-γ$^+$ T cells in unpaired samples of lung T_{RM}^{103+} cells ($n = 4$ samples) and blood T_{EM} cells or naive T cells (T_N cells) ($n = 2$ samples each) stimulated for various times (horizontal axis) with PMA and ionomycin in the presence of brefeldin A. (**j**,**k**) Flow cytometry (**j**) and quantification (**k**) of PD-1 expression in paired samples ($n = 9$) of lung T_{RM}^{103+} and blood T_{EM} cells (key in **k**; lines connect paired samples). Each symbol (**a**,**b**,**e**,**f**,**h**,**i**) represents an individual donor; small horizontal lines indicate the mean (± s.d. in **b**,**f**,**i**). *FDR < 0.05, **FDR < 0.01 and ***FDR < 0.001 (**a**,**b**,**e**,**f**,**h**,**i**). *$P < 0.05$ and **$P < 0.01$ (paired *t*-test (**c**,**d**,**k**) or two-way analysis of variance (ANOVA) with the Bonferroni post-hoc test (**g**)). Data are representative of one experiments (**a**,**b**,**e**,**f**,**h**,**i**), nine experiments (**c**,**d**,**j**,**k**) or three experiments (**g**; mean ± s.d.).

and low expression, respectively, of *ITGAE* and *SELL* (**Fig. 3c**), lung T_{RM}^{103+} cells had high expression of the adhesion-molecule-encoding genes *ITGAV*, *CD44*, *CD97*, *VCAM1* and *CLDN18* (**Fig. 3d**). Thus, the lung T_{RM}^{103+} cells displayed patterns of chemokine receptors and adhesion molecules that clearly differed from those on circulating cells, consistent with their unique tissue localization.

Constitutive expression of effector-molecule-encoding genes

As a first line of defense, lung T_{RM} cells must act without delay to prevent respiratory pathogens from establishing a foothold. Notably, lung T_{RM} cells had constitutively high expression of mRNAs encoding effector molecules, such as granzyme B, IFN-γ and TNF, without the need for *in vitro* stimulation (**Fig. 4a**,**b**). The amounts of these

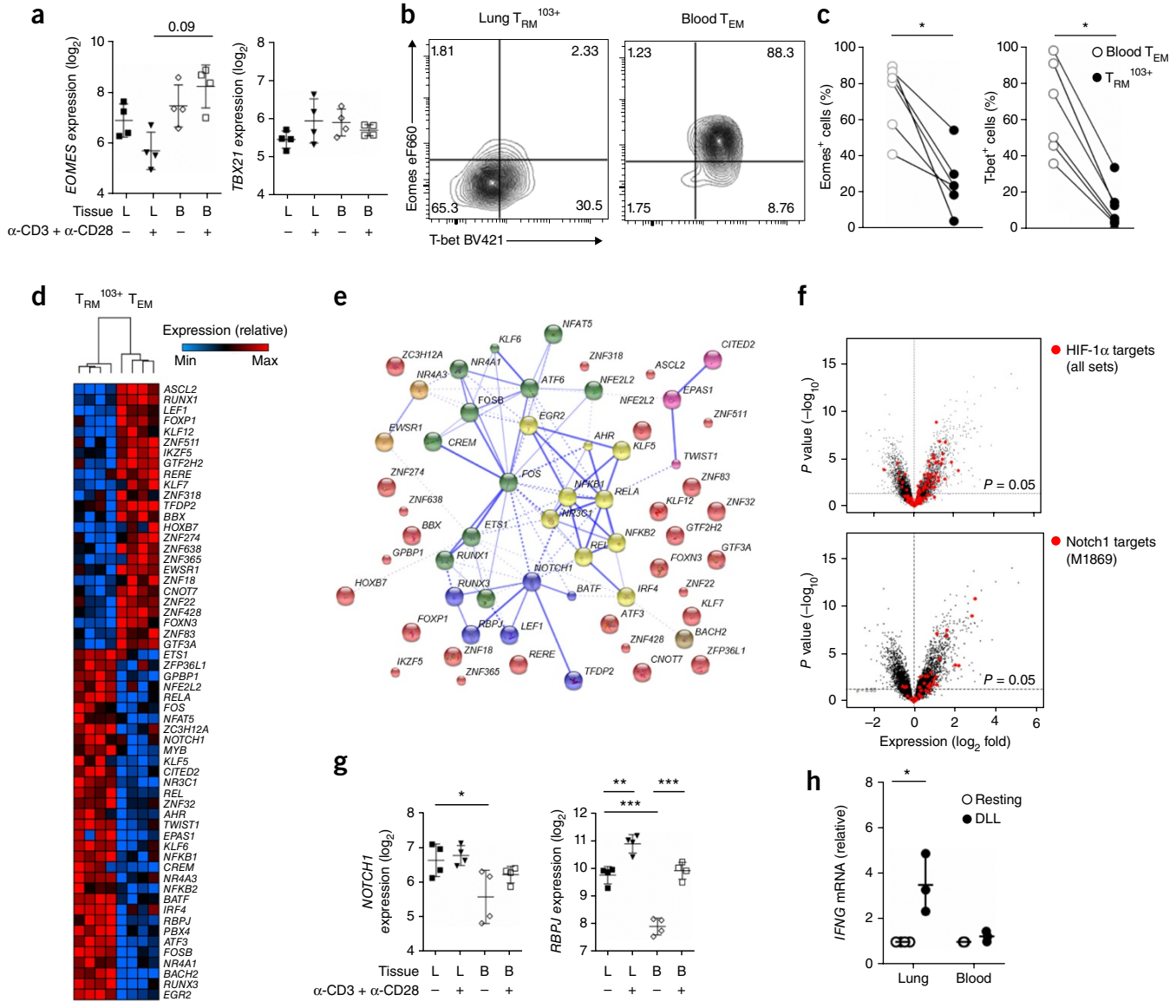

Figure 5 The transcription-factor circuitry of lung T_{RM}^{103+} cells. (**a**) Expression (log_2-transformed normalized values) of genes encoding eomesodermin (*EOMES*) and T-bet (*TBX21*) in lung- and blood-derived T cell subsets under resting conditions or after stimulation with anti-CD3 plus anti-CD28 (below plots). Number above bracketed line indicates FDR value. (**b**,**c**) Flow cytometry (bi-exponential scale) (**b**) and quantification (**c**) of the expression of eomesodermin (Eomes) and T-bet in paired samples ($n = 6$) of lung T_{RM}^{103+} cells and blood T_{EM} cells (lines (**c**) connect paired samples). (**d**) Expression (key) of mRNA encoding 58 transcription factors (right margin) differentially expressed in lung T_{RM}^{103+} cells versus blood T_{EM} cells under resting conditions; brackets above indicate hierarchical clustering. (**e**) Network analysis of the 58 transcription factors expressed differentially by lung T_{RM}^{103+} cells relative to their expression by blood T_{EM} cells, showing the transcription-factor complexes of AP-1 (green), Notch1-RBPJ (blue) and NF-κB (yellow). (**f**) Differential gene expression by lung T_{RM}^{103+} cells versus blood $CD8^+$ T cells for all probes (black) and gene sets (keys) that are targets of HIF-1α (MSigDB gene sets M2513, M12299, M255 and M6189, combined; top) or Notch1 (MSigDB gene set M1869; bottom), plotted against *P* values. (**g**) Expression (as in **a**) of *NOTCH1* and *RBPJ* in lung- and blood-derived T cell subsets under resting conditions or after stimulation with anti-CD3 plus anti-CD28 (below plots). *FDR < 0.05, **FDR < 0.01 and ***FDR < 0.001. (**h**) Quantitative PCR analysis of *IFNG* mRNA in lung T_{RM}^{103+} cells and blood T_{EM} cells (horizontal axis) after 4 h of rest or stimulation with plate-bound DLL1 and DLL4 (DLL) (key); results are normalized to those of mRNA encoding the mitochondrial ribosomal protein S18 and are presented relative to those obtained in the resting condition. Each symbol (**a**,**c**,**g**,**h**) represents an individual donor; small horizontal lines (**a**,**g**,**h**) indicate the mean (± s.d.). *$P < 0.05$ (paired *t*-test (**c**) or unpaired *t*-test (**h**)). Data are representative of one experiment (**a**,**d**–**g**), nine experiments (**b**,**c**), or two experiments with three independent donors (**h**).

Table 2 Transcription factors with target gene sets showing significant enrichment

Gene	Product	Enriched MsigDB gene set(s)	*P* value
HIF1A	Hypoxia-inducible factor 1α	M2513, M12299, M255, M6189	9.6×10^{-5}, 1.5×10^{-4}, 5.5×10^{-4}, 9.0×10^{-4}
NOTCH1	Notch homolog 1, translocation-associated	M1869, M14560	1.1×10^{-4}, 2.2×10^{-3}
NFKB1	NF-κB1	M8804, M1171, M11921, M1983	1.3×10^{-4}, 1.6×10^{-4}, 1.5×10^{-3}, 7.4×10^{-3}
ATF3	Activating transcription factor 3	M13967	2.2×10^{-4}
STAT5A	Signal transducer and activator of transcription 5A	M2216, M4372	2.8×10^{-4}, 1.6×10^{-3}
STAT3	Signal transducer and activator of transcription 3	M2312, M1163	3.8×10^{-4}, 3.4×10^{-3}
IRF4	Interferon regulatory factor 4	M11189, M12037	7.5×10^{-4}, 1.6×10^{-3}
CEBPB	CCAAT/enhancer binding protein-β	M12338	8.6×10^{-4}
EGR2	Early growth response 2	M12804	2.1×10^{-3}
MYC	c-Myc	M11290	2.3×10^{-3}
FOXO1	Forkhead box O1	M11512	2.6×10^{-3}
MYB	c-Myb	M863	2.9×10^{-3}

Twelve transcription factors for which one or more target gene sets showed significant enrichment in lung T_{RM} cells versus blood cells.

transcripts in resting lung T_{RM}^{103+} cells were as high as those reached in circulating T_{EM} cells after activation via the TCR and CD28 (**Fig. 4b**). Notably, resting lung T_{RM}^{103+} cells had little expression of these effector molecules at the protein level[17] (**Fig. 4c**,**d**), unlike blood T_{EM} cells, which, for example, clearly had granzyme B protein, despite their much lower constitutive expression of mRNA encoding granzyme B (**Fig. 4b**–**d**). Lung T_{RM} cells thus maintained large amounts of mRNA without accumulating protein.

An important function of T_{RM} cell–derived IFN-γ is to induce the secretion of chemokines by epithelial cells[11,22]. We found that lung T_{RM}^{103+} cells themselves also expressed genes encoding many chemokines (**Fig. 4e**,**f**), which might contribute to this sense-and-alarm function. Thus, lung T_{RM}^{103+} cells had constitutively elevated expression of the chemokine-encoding genes *CCL3*, *CCL4*, C*CL20* and *XCL1* (**Fig. 4e**,**f**). Regulation varied among the chemokines. Expression of the gene encoding CCL3, an attractant for macrophages, $CD4^+$ T cells and $CD8^+$ T cells, was (further) induced by the activation via the TCR and CD28 on T_{RM}^{103+} cells, whereas the expression of genes encoding other chemokines, such as CCL20, was hardly induced at all or was even reduced (**Fig. 4e**,**f**).

The expression of deployment-ready mRNAs encoding effector molecules could save precious time, which might make the difference between containment of microbes in the upper airways and full-blown infection. Indeed, lung T_{RM}^{103+} cells secreted IFN-γ more rapidly than blood-derived T cells did after *in vitro* stimulation with the phorbol ester PMA and ionomycin (**Fig. 4g**), as found for murine airway $CD8^+$ T cells[23].

Despite such robust effector function, lung T_{RM}^{103+} cells simultaneously expressed genes encoding inhibitory molecules, such as CTLA4, BTLA, LAG3, SPRY1 and the adenosine receptor A2AR (**Fig. 4h**,**i**). Furthermore, most of these cells were PD-1^{hi} (**Fig. 4j**,**k**). Finally, lung T_{RM}^{103+} cells had higher expression of transcription factors that inhibit effector function, such as TWIST1 and BACH2, than that of blood T_{EM} cells[24,25] (**Supplementary Fig. 5**). While seemingly at odds with the requisite vigilance of T_{RM}^{103+} cells, expression of all these inhibitors might impose a degree of restraint to help prevent unnecessary loss of tissue integrity upon infection.

Transcription factors that define T_{RM} cells

Given their constitutive expression of mRNAs encoding effector molecules, we expected that lung T_{RM}^{103+} cells would have abundant expression of factors that drive the transcription of these mRNAs. However, two major regulators of such genes, T-bet and eomesodermin[26], were not expressed in lung T_{RM}^{103+} cells (**Fig. 5a–c**), as reported for mouse skin-resident T cells[27]. To search for candidates that might control constitutive expression of effector-molecule-encoding genes, we analyzed the expression patterns of transcription factors. We found that 58 transcription factors had differential expression in lung-derived T cells relative to that in circulating T_{EM} cells (**Fig. 5d**). Many of these factors fell into interconnected clusters in a protein-association network; these included the activator protein AP-1, Notch1-RBPJ (RBPJ is also known as CSL) and NF-κB transcription-factor complexes (**Fig. 5e**). We found that 33 transcription factors had higher expression in lung-derived memory T cells than in circulating T_{EM} cells (**Fig. 5d**). Among these were RUNX3, which might regulate CD103 expression[28], as well as BATF and AHR, which regulate the expression of homing receptors and the maintenance of mouse T_{RM} cells, respectively[29,30] (**Fig. 5d** and **Supplementary Fig. 5**). The transcription factors Hobit (ZNF683) and BLIMP1 (encoded by *PRDM1*), identified as master regulators of T_{RM} cells in mice[31], were not expressed differentially by lung T_{RM}^{103+} cells relative to their expression by circulating T_{EM} cells, because the latter population, unlike their mouse counterpart[31], also expressed Hobit and BLIMP1 (ref. 32) (**Supplementary Fig. 5**).

Many of the transcription factors with high expression in lung T_{RM}^{103+} cells are known drivers of effector function, including RUNX3, ETS1, EPAS1, IRF4, various members of the NF-κB family (NF-κB1, REL, NF-κB2, NFAT5 and RELA) and Notch1 (ref. 33). The idea that many of these transcription factors were biologically active in lung T_{RM} cells was supported by gene-set–enrichment analysis of target genes through the use of CAMERA, in which we searched for transcription-factor 'fingerprints' within the regulatory regions of genes with higher expression in lung T_{RM} cells than in blood T_{EM} cells (**Table 2**). The most significantly enriched gene sets in this analysis were those that contain targets of the transcription factors HIF-1α and Notch1 (**Fig. 5f** and **Supplementary Table 2**), which are both promoters of T cell effector function[34–37].

Notch is a cell-surface receptor that is cleaved by a γ-secretase after ligand-induced activation, which allows its intracellular domain to migrate to the nucleus. There, the intracellular domain of Notch acts as a transcriptional activator by associating with the DNA-binding factor CSL (encoded by *RBPJ*). *RBPJ* was among the genes expressed most differentially by lung T_{RM}^{103+} cells relative to their expression by blood T_{EM} cells; its mRNA was present at much higher levels in T_{RM}^{103+} cells than in blood T_{EM} cells (**Fig. 5g**). Expression of *NOTCH1* was also high in lung T_{RM}^{103+} cells (**Fig. 5g**). As Notch transactivates the gene encoding IFN-γ (*Ifng*) in mice[38], we investigated whether activation of this pathway would elicit the expression of *IFNG* in human lung $CD8^+$ T_{RM} cells. Culture of lung T_{RM} cells *in vitro* resulted in a decrease in the steady-state abundance of *IFNG* mRNA (data not shown), consistent with a requirement for external signal input. Stimulation of these cells with recombinant Delta-like ligands (DLLs), which activate Notch signaling, resulted in higher

expression of *IFNG* mRNA than that of mock-stimulated control cells (**Fig. 5h**). Notably, this induction did not require stimulation through the TCR (**Fig. 5h**). These results suggested that Notch contributed to maintenance of constitutive *IFNG* expression in lung T_{RM} cells.

Control of the number of T_{RM}^{103+} cells by Notch

How T_{RM} cells are maintained is not clear. Notch has been linked to the maintenance of $CD4^+$ memory T cells[39,40]. As T_{RM}^{103+} cells exhibited an active Notch signaling signature, we hypothesized that Notch might also serve to maintain T_{RM}^{103+} cells *in situ* in the tissue. A core T_{RM}^{103+} cell gene-expression signature has been determined in mouse T cells[8]. That signature was strongly conserved in human T_{RM}^{103+} cells (**Fig. 6a** and **Supplementary Fig. 7**), which indicated that mice were a suitable model for determining the function of Notch in the T_{RM}^{103+} cell subset. Indeed, like their human counterparts, mouse lung T_{RM} cells (identified here on the basis of expression of CD69) also had higher expression of RBPJ than that of $CD69^-$ CD8 T cells from the lungs (**Fig. 6b**). Consistent with a possible function for the Notch pathway here, T_{RM}^{103+} cells from mouse lungs exhibited surface expression of Notch molecules, especially of Notch2 (**Supplementary Fig. 8a**). Furthermore, ligands for Notch were expressed by cell types expected to make contact with lung T_{RM} cells, including a subpopulation of $CD31^-CD326^+$ lung epithelial cells and $CD11b^+$ lung dendritic cells (**Supplementary Fig. 8b**). The necessary components therefore seemed to be in place to activate Notch in T_{RM}^{103+} cells in the lung tissue.

To study the function of Notch in lung T_{RM}^{103+} cells, we inactivated *Notch1* and *Notch2*, which often compensate for each other[37], in both $CD4^+$ T cells and $CD8^+$ T cells. To this end, we crossed mice carrying *lox*P-flanked *Notch1* and *Notch2* alleles (*Notch1*$^{fl/fl}$*Notch2*$^{fl/fl}$) with mice with transgenic expression of Cre recombinase from the T cell–specific gene *Cd4* (*Cd4*-Cre)[36], a setting that does not overtly affect T cell development[36]. We intravenously injected fluorescence-labeled antibodies to CD8β into the resultant mice briefly before sacrificing them, to allow unequivocal discrimination between $CD8^+$ T cells in blood (labeled with the antibody) and those that reside in the lung tissue (not labeled)[41]. Lungs from *Notch1*$^{fl/fl}$*Notch2*$^{fl/fl}$*Cd4*-Cre^+ mice had considerably fewer T_{RM}^{103+} cells than did those from their *Notch1*$^{fl/fl}$*Notch2*$^{fl/fl}$*Cd4*-Cre^- littermates (**Fig. 6c,d**), although the overall frequency of $CD8^+$ T cells in these lungs was similar in both groups of mice (**Supplementary Fig. 8c**). Furthermore, the average surface expression of CD103 by those remaining T_{RM}^{103+} cells was also lower in *Notch1*$^{fl/fl}$*Notch2*$^{fl/fl}$*Cd4*-Cre^+ mice than in their *Notch1*$^{fl/fl}$*Notch2*$^{fl/fl}$*Cd4*-Cre^- littermates (**Fig. 6c,e**).

To study the role of Notch in antigen-specific T_{RM}^{103+} cells, we infected mice intranasally with influenza A virus, strain HKx31 (H3N2). After 10 d, we sacrificed the mice and measured total $CD8^+$ T cells as well as $CD8^+$ T cells that bound the influenza-virus-specific tetramer of H-$2D^b$ and an epitope of amino acids 366–374 of influenza virus nucleocapsid protein (NP(366–374)). There was a distinctly lower frequency of the overall T_{RM}^{103+} cell population (**Fig. 6f**) as well as of the H-$2D^b$–NP(366–374)-tetramer-binding T_{RM}^{103+} cell population (**Fig. 6g**), in the *Notch1*$^{fl/fl}$*Notch2*$^{fl/fl}$*Cd4*-Cre^+ mice than in their *Notch1*$^{fl/fl}$*Notch2*$^{fl/fl}$*Cd4*-Cre^- littermate controls. Thus, Notch controlled either the generation or the maintenance of T_{RM}^{103+} cells in the lungs of mice.

Control of the maintenance of T_{RM}^{103+} cells by Notch

The Notch signature in the T_{RM} cell transcriptome suggested that this pathway is active in T_{RM} cells *in situ* in the lungs, consistent with the hypothesis that Notch signaling has a role in maintenance of

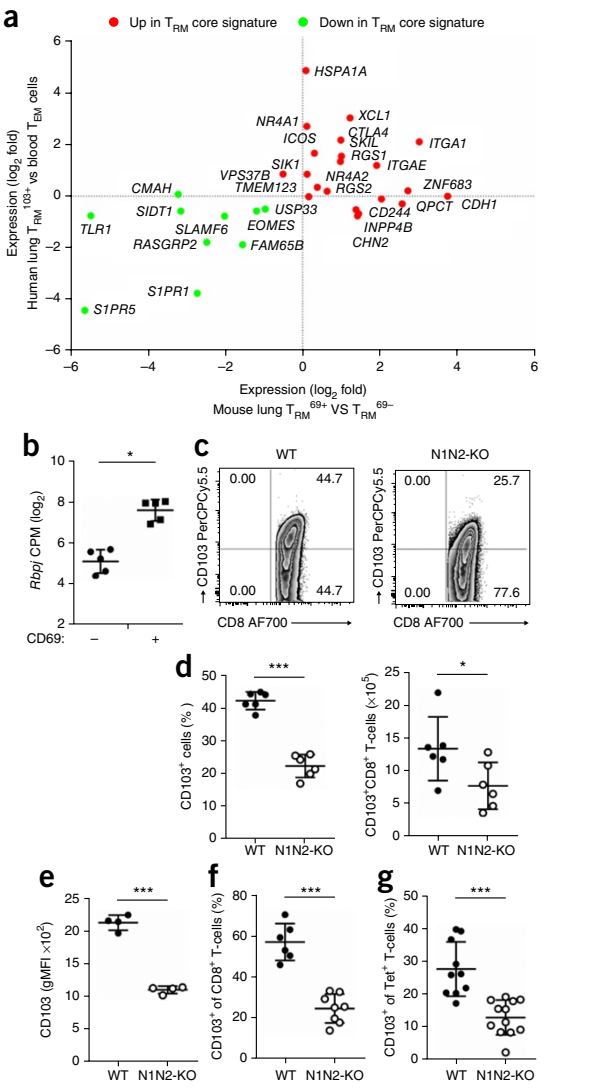

Figure 6 Notch controls the number of lung T_{RM}^{103+} cells. (**a**) Expression (log_2 fold values) of a minimal core signature of T_{RM} cells[8] for human lung T_{RM}^{103+} cells and mouse lung $CD69^+$ $CD8^+$ (T_{RM}^{69+}) cells (RNA sequencing of T_{RM}^{69+} cells from the lungs of wild-type mice), including genes with higher (Up) or lower (Down) expression in mouse T_{RM} cells than in splenic T cells[8] (key). (**b**) Expression (log_2 counts per million (CPM) normalized values) of *Rbpj* in paired samples ($n = 5$) of lung $CD8^+$ $CD69^-$ T cells and $CD69^+$ T cells (horizontal axis) under resting conditions. *FDR < 0.01. (**c**) CD103 expression by lung $CD8^+$ T cells from *Notch1*$^{fl/fl}$*Notch2*$^{fl/fl}$*Cd4*-Cre^+ mice (N1N2-KO) and *Notch1*$^{fl/fl}$*Notch2*$^{fl/fl}$*Cd4*-Cre^- mice (WT), under steady-state conditions. (**d**) Frequency (left) and absolute number (right) of CD103-expressing ($CD103^+$) lung $CD8^+$ T cells (protected from labeling with anti-CD8β) obtained from mice as in **c** ($n = 6$ per group), assessed by flow cytometry. (**e**) Geometric mean fluorescence intensity of CD103 in $CD103^+$ cells from mice as in **c** ($n = 4$ per genotype). (**f**) Frequency of $CD103^+$ $CD8^+$ T cells in the lungs of *Notch1*$^{fl/fl}$*Notch2*$^{fl/fl}$*Cd4*-Cre^+ mice ($n = 8$) and *Notch1*$^{fl/fl}$*Notch2*$^{fl/fl}$*Cd4*-Cre^- mice ($n = 6$) 10 d after intranasal infection with influenza virus strain HKx31. (**g**) Frequency of CD103-expressing ($CD103^+$) $CD8^+$ T cells specific for the influenza A virus NP(366–374) tetramer (Tet^+) in *Notch1*$^{fl/fl}$*Notch2*$^{fl/fl}$*Cd4*-Cre^+ mice ($n = 12$) and *Notch1*$^{fl/fl}$*Notch2*$^{fl/fl}$*Cd4*-Cre^- mice ($n = 10$) 10 d after intranasal infection with HKx31. Each symbol (**b**,**d**,**e**–**g**) represents an individual donor; small horizontal lines indicate the mean (± s.d.). $^*P < 0.05$, $^{**}P < 0.01$ and $^{***}P < 0.001$ (unpaired *t*-test). Data are representative of one experiment (**a**), three experiments (**b**,**g**), three experiments with six independent stainings (**c**) or two experiments (**d**–**f**).

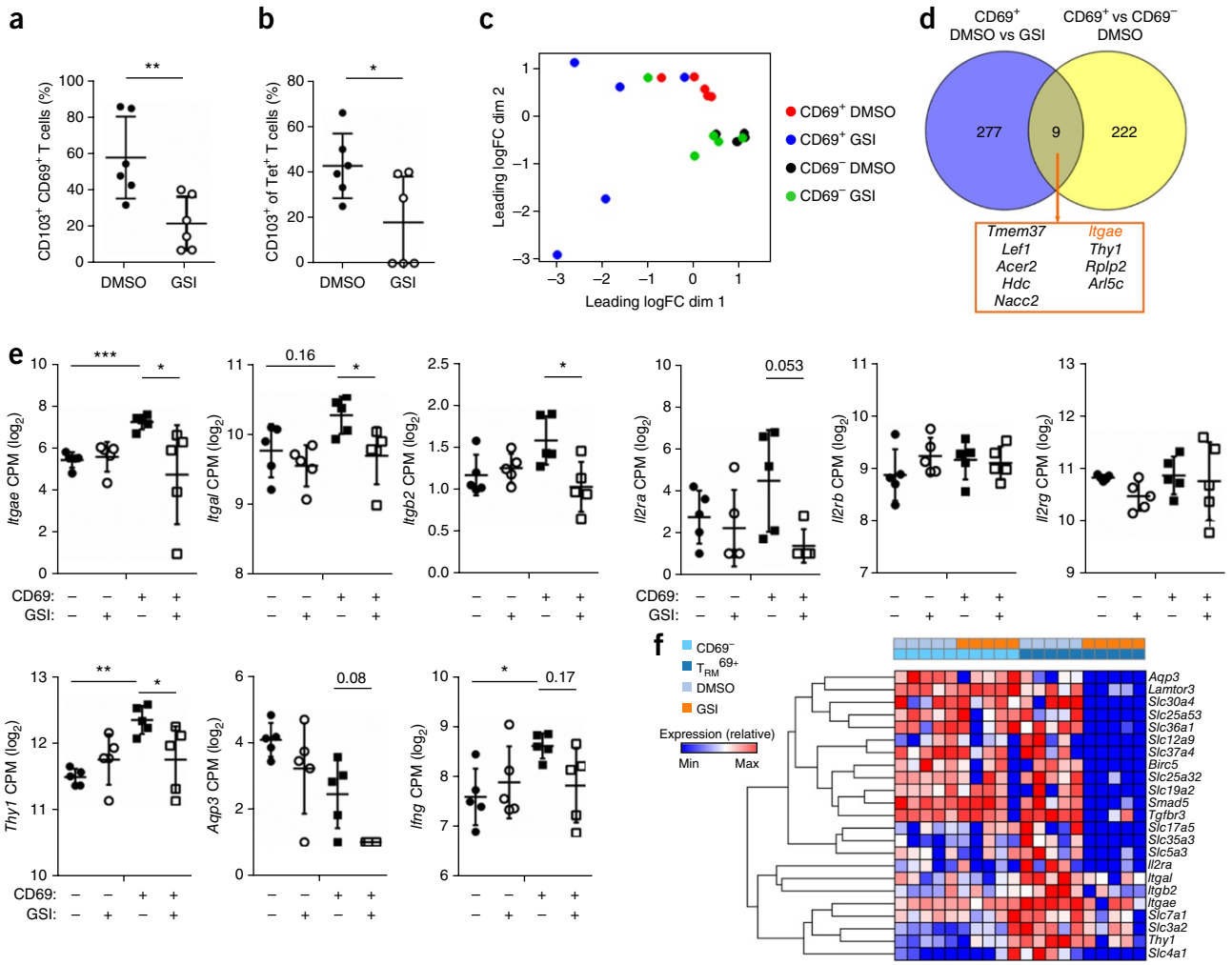

Figure 7 Notch controls the maintenance of T_{RM}^{103+} cells. (**a**) Frequency of CD103$^+$ CD8$^+$ T cells among CD69$^+$ T cells (protected from labeling by intravenously injected anti-CD8β) in wild-type mice ($n = 5$ per group) infected with influenza virus HKx31 and, 35 d later, treated for 5 d with the vehicle DMSO or GSI. (**b**) Frequency of CD103-expressing (CD103$^+$) CD8$^+$ T cells specific for the influenza A virus NP(366–374) tetramer (Tet$^+$) in mice as in **a**. (**c**) Multi-dimensional scaling analysis (of RNA-sequencing results) of lung CD69$^+$ and CD69$^-$ CD8$^+$ T cell populations (key) sorted from mice infected with influenza virus HKx31 and, 35 d later, treated for 2 d with DMSO or GSI (key), presented as 'leading fold change' (logFC) in the first dimension (dim1) and second dimension (dim2), which represent the elements of the data that constitute the greatest difference between samples (indicative of the degree of sample relatedness). (**d**) Genes differentially expressed by CD69$^+$ memory CD8$^+$ T cells from the lungs of mice as in **c** treated with DMSO versus those treated with GSI (CD69$^+$ DMSO vs GSI) and by CD69$^+$ memory CD8$^+$ T cells versus CD69$^-$ memory CD8$^+$ T cells from DMSO-treated mice (CD69$^+$ versus CD69$^-$ DMSO), and the overlap of those groups (middle and bottom). FDR < 0.05. (**e**) Expression (as in **Fig. 6b**) of genes (vertical axes) in lung T cell subsets (key) obtained from mice pre-infected with influenza virus and treated for 2 d with DMSO or GSI (key) as in **c**. *FDR < 0.05, **FDR < 0.01 and ***FDR < 0.001. (**f**) Expression (key) of mRNA from various genes (right margin) in CD69$^-$ memory CD8$^+$ T cells (CD69$^-$) or T_{RM}^{69+} cells (T_{RM}^{69+}) from mice as in **c** (key, and above plot); brackets (left margin) indicate hierarchical clustering. Each symbol (**a**,**b**,**e**) represents an individual donor; small horizontal lines indicate the mean (± s.d.). *$P < 0.05$, **$P < 0.01$ and ***$P < 0.001$ (unpaired *t*-test (**a**,**b**)). Data are representative of two experiments (**a**,**b**) or one experiment (**c**–**f**).

T_{RM} cells. To investigate this, we first induced a population of lung T_{RM} cells by intranasally infecting wild-type mice with influenza virus. After 35 d, we treated mice with γ-secretase inhibitor (GSI) or vehicle for 5 continuous days to block Notch signaling in already established T_{RM} cells. Treatment with GSIs resulted in a significant decrease in T_{RM}^{103+} cells in the total and H-2D^b–NP(366–374)-tetramer-binding populations (**Fig. 7a,b**). These results demonstrated that Notch signaling was required for the persistence of T_{RM}^{103+} cells.

To understand how Notch carries out that function, we performed whole-transcriptome analysis of memory T cell populations isolated from mice treated with GSI. To avoid a negative bias due to (possible) loss of CD103$^+$ cells and consequent selection for the remaining cells not affected by GSI treatment, we assessed the gene-expression profiles of the total CD69$^+$ population, in which the T_{RM}^{103+} cell signature was readily detectable (**Fig. 6a**). Loss of T_{RM}^{103+} cells after treatment with GSI should be reflected by a global reduction in the T_{RM}^{103+} cell gene-expression signature within the transcriptome of CD69$^+$ cells. We furthermore limited the treatment to 48 h to capture gene-expression changes before most of the T_{RM}^{103+} cells were lost (**Supplementary Fig. 8d**). Multidimensional scaling analysis showed that GSI treatment prominently affected gene expression in CD69$^+$ lung memory T cells but not in the CD69$^-$ population (**Fig. 7c**). Inhibition of Notch affected expression of only a few T_{RM} cell–specific genes (**Fig. 7d**). Most notable among these was *Itgae* (**Fig. 7e**), consistent with the lower surface intensity of CD103 on T_{RM} cells from *Notch1*$^{fl/fl}$*Notch2*$^{fl/fl}$*Cd4*-Cre$^+$ mice than on those from *Notch1*$^{fl/fl}$*Notch2*$^{fl/fl}$*Cd4*-Cre$^-$ mice (**Fig. 6e**).

Table 3 Enriched gene sets affected by GSI treatment

Gene set name	Total genes in set	Gene symbols	FDR
Myc targets	14	*Mcm4*, *Nop56*, *Ctps*, *Odc1*, *Cdc45*, *Eprs*, *Ywhae*, *Phb2*, *Tyms*, *Uba2*, *Fbl*, *Exosc7*, *Ppm1g*, *Ube2l3*	4.5×10^{-7}
Cell-cycle-related E2F targets	13	*Mcm4*, *Nop56,Ctps*, *Birc5*, *Stmn1*, *Stag1*, *Suv39H1*, *Nbn*, *Cse1l*, *Lyar*, *Asf1b*, *Prkdc*, *Rqcd1*	1.8×10^{-6}
p53 pathway	12	*Slc19a2*, *Sat1*, *Tsc22d1*, *Ldhb*, *Ptpre*, *Plk2*, *Trafd1*, *Adck3*, *Rrp8*, *Pitpnc1*, *Osgin1*, *Slc3a2*	9.1×10^{-6}
G2M checkpoint	11	*Odc1*, *Cdc45*, *Birc5*, *Stmn1*, *Stag1*, *Suv39h1*, *Ccnf*, *Incenp*, *Kif11*, *Slc7a1*, *Chaf1a*	3.8×10^{-5}
mTORC1 signaling	11	*Mcm4*, *Eprs*, *Ccnf*, *Apt2a2*, *Glrx*, *Slc37a4*, *Atp6vid*, *Txnrd1*, *Itgb2*, *Mllt11*, *Pitpnb*	3.8×10^{-5}
Estrogen early response	9	*Slc19a2*, *Abhd2*, *Igf1r*, *Aqp3*, *Olfm1*, *Ablim1*, *Inpp5f*, *Kdm4b*, *Isg20l2*	8.4×10^{-4}
Mitotic spindle assembly	9	*Ywhae*, *Birc5*, *Incenp*, *Kif11*, *Tubgcp3*, *Sass6*, *Rabgap1*, *Cep192*, *Arap3*	8.4×10^{-4}
Androgen response	6	*Sat1*, *Tsc22d1*, *Abhd2*, *Akt1*, *Abcc4*, *Camkk2*	2.3×10^{-3}
Glycolysis	8	*Stmn1*, *Glrx*, *Slc37a4*, *Ak3*, *B3galt6*, *Znf292*, *Pgm2*, *Slc35a3*	2.9×10^{-3}
Oxidative phosphorylation	8	*Phb2*, *Ldhb*, *Atp6v1d*, *Dlts*, *Supv3l1*, *Dlat*, *Mtx2*, *Cox11*	2.9×10^{-3}
Fatty acid metabolism	7	*Odc1*, *Nbn*, *Dlst*, *Cpox*, *Hsd17b4*, *Acadl*, *Mcee*	3.1×10^{-3}
IL-2 STAT5 signaling	7	*Odc1*, *Igf1r*, *Map3k8*, *Il2ra*, *S100a1*, *Itgae*, *Twsg1*	9.9×10^{-3}
DNA repair	6	*Tyms*, *Ak3*, *Zwint*, *Ercc8*, *Smad5*, *Rad51*	9.9×10^{-3}
Interferon-γ response	6	*Trafd1*, *Il15ra*, *Irf9*, *Dhx58*, *Pnpt1*, *Klrk1*	2.5×10^{-2}
Apoptosis	5	*Sat1*, *Psen2*, *Lef1*, *Tgfbr3*, *Casp9*	3.4×10^{-2}

Fifteen prominent enriched gene sets affected in $CD69^+$ cells by treatment of mice with GSI.

Although Notch activation induced expression of *IFNG* in human T_{RM} cells, expression of *Ifng* in mouse cells was not significantly inhibited, despite a downward trend (**Fig. 7e**).

The large majority of the 277 genes affected by GSI treatment did not belong to the T_{RM} cell–specific transcriptome (**Fig. 7d**). These genes included known Notch targets, such as *Il2ra* (**Fig. 7e**). Expression of *Il2rb* and *Il2rg* (which encode the receptor for IL-15) was not affected by GSI treatment (**Fig. 7e**). This finding was important, as signaling via the IL-15 receptor has been linked to the maintenance of T_{RM} cells[8,27]. Gene-set–enrichment analysis also revealed that GSI treatment affected processes such as signaling via the metabolic checkpoint complex mTORC1 and glycolysis (**Table 3**), which have previously been linked to Notch signaling in T cells[37]. Closer examination of specific genes showed that several genes encoding products in the integrin signaling pathway (*Itgal, Itgb2* and *Thy1*) were downregulated, in addition to *Itgae* (**Fig. 7e**). Notable was also the downregulation of a large number of genes encoding transporters for amino acids (*Slc36a1*, *Slc7a1* and *Slc3a2*), metabolites (*Slc12a9*, *Slc30a4* and *Slco4a1*), trace elements and ions (*Slc12a9*, *Slc30a4* and *Slc4a1*), and metabolites and nutrients (*Slc37a4*, *Slc25a32*, *Slc19a2* and *Aqp3*) (**Fig. 7f**). These results suggested that a major function for Notch signaling is to control metabolic programs in T_{RM} cells, a hypothesis further reinforced by the enrichment, within the Notch dependent transcriptome, for multiple gene sets associated with metabolism, including glycolysis, oxidative phosphorylation and fatty acid metabolism (**Table 3**).

DISCUSSION

The respiratory tract is a front line where immune cells must promptly ward off pathogens but avoid excessive damage to the delicate lung tissues. Our data have demonstrated specialized features of lung $CD8^+$ T_{RM}^{103+} cells that equip them for this balancing act. First among these was their eponymous anatomical localization, reflected by the distinct expression of genes encoding products associated with migration and adhesion. Expression of the chemokine receptor CCR6 stood out in T_{RM}^{103+} cells. This receptor is responsive to CCL20 produced by lung epithelial cells and, in a potential positive feedback loop, by lung T_{RM} cells themselves. The CCR6–CCL20 axis is, however, not restricted to the respiratory tract[42]. A receptor that might help determine lung tropism is CXCR6, as its ligand, CXCL16, has high expression by lung epithelial cells[43]. A second specialization was their constitutive expression of deployment-ready mRNAs encoding pro-inflammatory cytokines and cytotoxic mediators, which would presumably prevent delays required for transcription. Indeed, lung T_{RM} cells rapidly produce IFN-γ after *in vitro* stimulation[23]. T_{RM} cells recruit auxiliary immune cells via IFN-γ-mediated induction of chemokine production by epithelial cells[11]. Interestingly, human lung T_{RM}^{103+} cells themselves expressed multiple chemokine-encoding genes, which would possibly allow more expeditious recruitment of auxiliary troops than would indirect production of chemokines by epithelial cells. Despite their constitutive mRNA expression, resting lung T_{RM}^{103+} cells did not have the corresponding effector proteins[17]. This suggests that a mechanism exists to translate such mRNAs into proteins only when justified by TCR activation. The poised effector program in T_{RM}^{103+} cells was accompanied by a gene-expression program associated with inhibition of T cell activation, including genes encoding inhibitory receptors (*CTLA4*, *BTLA4* and *KLRC1)*, suppressive transcription factors (*BACH2* and *TWIST1*) and an inhibitor of TCR signaling (*SPRY1*). Although apparently at odds with the vigilance required of T_{RM}^{103+} cells, these inhibitory modules might impose restraint to prevent immunopathology from excessive immunoreactivity.

How is constitutive expression of mRNAs encoding effector molecules maintained? Constitutive transcription probably contributes to this, independently of agonist-peptide-driven TCR stimulation. Although T_{RM} cells expressed little T-bet and eomesodermin[27], other regulators of genes encoding effector molecules (for example, *NOTCH*, *HIF1A*, *IRF4* and *NFKB*) were active in these cells. Activity of HIF-1α, a transcription factor that operates in response to hypoxia, seems inconsistent with the high oxygen tension in the lungs. Although we considered that hypoxia during sample processing might have affected our results, we believe this is unlikely. First, such a signature was not observed in lung $CD4^+$ T_{RM} cells isolated in parallel (A.O., R.A.v.L. and P.H., data not shown). Furthermore, lung T_{RM}^{103+} cells had higher expression of both *HIF1A* mRNA and *HIF2A* mRNA than that of blood T_{EM} cells, whereas hypoxia controls this pathway via the (post-translational) stabilization of proteins of the HIF family. Indeed, transcription factors of the HIF family also operate in T cells under normoxic conditions, and their expression is induced by cytokines or extracellular ATP[44,45].

Notch controls the effector differentiation and function of $CD8^+$ T cells[36,38]. We found that stimulation with DLL ligands elicited expression of *IFNG* mRNA in human lung T_{RM} cells. Nonetheless, short-term inhibition of Notch signaling in mice diminished the expression of *Ifng* mRNA only slightly. This finding suggests that these transcripts are very stable or that other transcription factors are sufficient to drive constitutive *Ifng* expression, at least in mice. Determination of the role of Notch in the control of effector-molecule-encoding genes during reinfection and in immunity to

pathogens awaits the generation of a system that allows inducible elimination of this pathway only in T_{RM} cells.

We found that Notch controlled the maintenance of T_{RM}^{103+} cells by multiple parallel mechanisms. Notch controlled maximal expression of CD103, which presumably helps to anchor T_{RM}^{103+} cells in epithelia[5]. Most of the T_{RM}^{103+} cell–specific gene-expression program, however, was independent of Notch. Expression of the adhesion molecules LFA1 (encoded by *Itgal* and *Itgb2*) and the glycoprotein Thy1 depended on Notch, but the consequences of this are not currently clear. Notch signaling controls the persistence of circulating memory $CD4^+$ T cells through the regulation of glucose metabolism[40,46]. However, the concentration of glucose is low in the lung mucosa[20], as emphasized by the prominent expression of genes associated with glucose starvation in human lung T_{RM} cells. Circulating memory $CD8^+$ T cells rely on the import of glycerol, which can be catabolized via the glycolytic pathway and subsequent oxidative phosphorylation[47]. Both these metabolic pathways were affected by inhibition of Notch in mouse T_{RM} cells, as was expression of the glycerol importer aquaporin-3. In addition, Notch regulated the expression of a series of other transporters for amino acids, trace elements and ions. Together these results suggest that Notch controls the maintenance of T_{RM}^{103+} cells at least in part by regulating basic metabolic functions.

Apart from Notch, the transforming growth factor-β (TGF-β) pathway has an important role in T_{RM}^{103+} cells[8,48]. Extensive crosstalk exists between these two pathways. TGF-β induces the expression of Notch ligands in epithelial cells, and the intracellular domain of Notch interacts with signal transducers of the Smad family, which are the effectors of the TGF-β pathway[49,50]. Secretion of TGF-β and expression of Notch ligands thus constitute an integrated mechanism by which the lung mucosal tissue actively maintains the T cell population that protects it from infectious assault.

There is growing appreciation of the clinical importance of tissue-specific T cell memory. We believe that apart from yielding novel insights into the biology of these cells, our study will serve as a valuable resource for further studies into local adaptive immune processes in lungs. Such studies will ultimately aid the development of strategies for vaccination against respiratory infections and possibly also for immunotherapy of cancers of the lung.

METHODS

Methods and any associated references are available in the online version of the paper.

Accession codes. GEO: human mRNA data, GSE61397 (MIAME-compliant format); mouse mRNA data, GSE79774.

Note: Any Supplementary Information and Source Data files are available in the online version of the paper.

ACKNOWLEDGMENTS

We thank K.P. Gisbergen and I.J. ten Berge for discussions; E. Mul and T. Poplonski for assistance with flow cytometry sorting; J. Kloek, M. Jonker, E. Hendriks, J. Weening, H. Stel, E. Prins, G. Nossent and E. Verschuuren for help with obtaining patient material; A. ten Brinke (Sanquin, Amsterdam) for tetramer reagents; and R. Lutter, B.S. Dierdorp and T. Dekker for coordinating technical assistance. Supported by the Landsteiner Stichting voor Bloedtransfusie Research (1136 to R.A.W.v.L.), the Netherlands Asthma Foundation (3.2.06.020 to R.A.W.v.L.), the Alexander von Humboldt Foundation (R.S.) and the Netherlands organization for scientific research (NWO-ALW; to D.A.).

AUTHOR CONTRIBUTIONS

P.H., C.H., H.C.C. and D.A. designed the experiments; P.H., C.H., R.A.B., B.P., A.E.O., R.S., G.B. and O.B. did the experiments; P.H., C.H., A.J., B.N. and P.D.M. analyzed the data; B.P. and R.E.J. contributed patient samples; R.A.W.v.L. initiated the research program and directed the study together with P.D.M. and D.A.; and P.H. and D.A. wrote the manuscript.

COMPETING FINANCIAL INTERESTS

The authors declare no competing financial interests.

1. Wu, T. *et al.* Lung-resident memory CD8 T cells (TRM) are indispensable for optimal cross-protection against pulmonary virus infection. *J. Leukoc. Biol.* **95**, 215–224 (2014).
2. Turner, D.L. *et al.* Lung niches for the generation and maintenance of tissue-resident memory T cells. *Mucosal Immunol.* **7**, 501–510 (2014).
3. Woodland, D.L. & Kohlmeier, J.E. Migration, maintenance and recall of memory T cells in peripheral tissues. *Nat. Rev. Immunol.* **9**, 153–161 (2009).
4. Sheridan, B.S. & Lefrançois, L. Regional and mucosal memory T cells. *Nat. Immunol.* **12**, 485–491 (2011).
5. Sathaliyawala, T. *et al.* Distribution and compartmentalization of human circulating and tissue-resident memory T cell subsets. *Immunity* **38**, 187–197 (2013).
6. Park, C.O. & Kupper, T.S. The emerging role of resident memory T cells in protective immunity and inflammatory disease. *Nat. Med.* **21**, 688–697 (2015).
7. Skon, C.N. *et al.* Transcriptional downregulation of S1pr1 is required for the establishment of resident memory $CD8^+$ T cells. *Nat. Immunol.* **14**, 1285–1293 (2013).
8. Mackay, L.K. *et al.* The developmental pathway for $CD103^+CD8^+$ tissue-resident memory T cells of skin. *Nat. Immunol.* **14**, 1294–1301 (2013).
9. Sheridan, B.S. *et al.* Oral infection drives a distinct population of intestinal resident memory $CD8^+$ T cells with enhanced protective function. *Immunity* **40**, 747–757 (2014).
10. Steinert, E.M. *et al.* Quantifying memory CD8 T cells reveals regionalization of immunosurveillance. *Cell* **161**, 737–749 (2015).
11. Ariotti, S. *et al.* T cell memory. Skin-resident memory CD8 T cells trigger a state of tissue-wide pathogen alert. *Science* **346**, 101–105 (2014).
12. Wilkinson, T.M. *et al.* Preexisting influenza-specific $CD4^+$ T cells correlate with disease protection against influenza challenge in humans. *Nat. Med.* **18**, 274–280 (2012).
13. Sridhar, S. *et al.* Cellular immune correlates of protection against symptomatic pandemic influenza. *Nat. Med.* **19**, 1305–1312 (2013).
14. Slütter, B., Pewe, L.L., Kaech, S.M. & Harty, J.T. Lung airway-surveilling $CXCR3^{hi}$ memory $CD8^+$ T cells are critical for protection against influenza A virus. *Immunity* **39**, 939–948 (2013).
15. Shay, T. *et al.* Conservation and divergence in the transcriptional programs of the human and mouse immune systems. *Proc. Natl. Acad. Sci. USA* **110**, 2946–2951 (2013).
16. den Braber, I. *et al.* Maintenance of peripheral naive T cells is sustained by thymus output in mice but not humans. *Immunity* **36**, 288–297 (2012).
17. Piet, B. *et al.* $CD8^+$ T cells with an intraepithelial phenotype upregulate cytotoxic function upon influenza infection in human lung. *J. Clin. Invest.* **121**, 2254–2263 (2011).
18. Akbulut, S. *et al.* Sprouty proteins inhibit receptor-mediated activation of phosphatidylinositol-specific phospholipase C. *Mol. Biol. Cell* **21**, 3487–3496 (2010).
19. Wu, D. & Smyth, G.K. Camera: a competitive gene set test accounting for inter-gene correlation. *Nucleic Acids Res.* **40**, e133 (2012).
20. Pezzulo, A.A. *et al.* Glucose depletion in the airway surface liquid is essential for sterility of the airways. *PLoS One* **6**, e16166 (2011).
21. Jung, S. *et al.* Analysis of fractalkine receptor CX_3CR1 function by targeted deletion and green fluorescent protein reporter gene insertion. *Mol. Cell. Biol.* **20**, 4106–4114 (2000).
22. Schenkel, J.M., Fraser, K.A., Vezys, V. & Masopust, D. Sensing and alarm function of resident memory $CD8^+$ T cells. *Nat. Immunol.* **14**, 509–513 (2013).
23. McMaster, S.R., Wilson, J.J., Wang, H. & Kohlmeier, J.E. Airway-resident memory CD8 T cells provide antigen-specific protection against respiratory virus challenge through rapid IFN-γ production. *J. Immunol.* **195**, 203–209 (2015).
24. Yang, M.H. *et al.* Direct regulation of TWIST by HIF-1a promotes metastasis. *Nat. Cell Biol.* **10**, 295–305 (2008).
25. Roychoudhuri, R. *et al.* BACH2 represses effector programs to stabilize T_{reg}-mediated immune homeostasis. *Nature* **498**, 506–510 (2013).
26. Intlekofer, A.M. *et al.* Effector and memory $CD8^+$ T cell fate coupled by T-bet and eomesodermin. *Nat. Immunol.* **6**, 1236–1244 (2005).
27. Mackay, L.K. *et al.* T-box transcription factors combine with the cytokines TGF-β and IL-15 to control tissue-resident memory T cell fate. *Immunity* **43**, 1101–1111 (2015).
28. Grueter, B. *et al.* Runx3 regulates integrin alpha E/CD103 and CD4 expression during development of $CD4^-/CD8^+$ T cells. *J. Immunol.* **175**, 1694–1705 (2005).
29. Li, Y. *et al.* Exogenous stimuli maintain intraepithelial lymphocytes via aryl hydrocarbon receptor activation. *Cell* **147**, 629–640 (2011).
30. Wang, C. *et al.* BATF is required for normal expression of gut-homing receptors by T helper cells in response to retinoic acid. *J. Exp. Med.* **210**, 475–489 (2013).
31. Mackay, L.K. *et al.* Hobit and Blimp1 instruct a universal transcriptional program of tissue residency in lymphocytes. *Science* **352**, 459–463 (2016).

32. Vieira Braga, F.A. *et al.* Blimp-1 homolog Hobit identifies effector-type lymphocytes in humans. *Eur. J. Immunol.* **45**, 2945–2958 (2015).
33. Kaech, S.M. & Cui, W. Transcriptional control of effector and memory CD8+ T cell differentiation. *Nat. Rev. Immunol.* **12**, 749–761 (2012).
34. Kuijk, L.M. *et al.* Notch controls generation and function of human effector CD8+ T cells. *Blood* **121**, 2638–2646 (2013).
35. Doedens, A.L. *et al.* Hypoxia-inducible factors enhance the effector responses of CD8+ T cells to persistent antigen. *Nat. Immunol.* **14**, 1173–1182 (2013).
36. Backer, R.A. *et al.* A central role for Notch in effector CD8+ T cell differentiation. *Nat. Immunol.* **15**, 1143–1151 (2014).
37. Amsen, D., Helbig, C. & Backer, R.A. Notch in T cell differentiation: all things considered. *Trends Immunol.* **36**, 802–814 (2015).
38. Bailis, W. *et al.* Notch simultaneously orchestrates multiple helper T cell programs independently of cytokine signals. *Immunity* **39**, 148–159 (2013).
39. Helbig, C. *et al.* Notch controls the magnitude of T helper cell responses by promoting cellular longevity. *Proc. Natl. Acad. Sci. USA* **109**, 9041–9046 (2012).
40. Maekawa, Y. *et al.* Notch controls the survival of memory CD4+ T cells by regulating glucose uptake. *Nat. Med.* **21**, 55–61 (2015).
41. Anderson, K.G. & Masopust, D. Editorial: Pulmonary resident memory CD8 T cells: here today, gone tomorrow. *J. Leukoc. Biol.* **95**, 199–201 (2014).
42. Esplugues, E. *et al.* Control of T_H17 cells occurs in the small intestine. *Nature* **475**, 514–518 (2011).
43. Day, C., Patel, R., Guillen, C. & Wardlaw, A.J. The chemokine CXCL16 is highly and constitutively expressed by human bronchial epithelial cells. *Exp. Lung Res.* **35**, 272–283 (2009).
44. Wang, R. *et al.* The transcription factor Myc controls metabolic reprogramming upon T lymphocyte activation. *Immunity* **35**, 871–882 (2011).
45. Mascanfroni, I.D. *et al.* Metabolic control of type 1 regulatory T cell differentiation by AHR and HIF1-α. *Nat. Med.* **21**, 638–646 (2015).
46. Wang, W. *et al.* Notch receptor-ligand engagement maintains hematopoietic stem cell quiescence and niche retention. *Stem Cells* **33**, 2280–2293 (2015).
47. Cui, G. *et al.* IL-7-induced glycerol transport and TAG synthesis promotes memory CD8+ T cell longevity. *Cell* **161**, 750–761 (2015).
48. Zavadil, J., Cermak, L., Soto-Nieves, N. & Böttinger, E.P. Integration of TGF-β/Smad and Jagged1/Notch signalling in epithelial-to-mesenchymal transition. *EMBO J.* **23**, 1155–1165 (2004).
49. Blokzijl, A. *et al.* Cross-talk between the Notch and TGF-β signaling pathways mediated by interaction of the Notch intracellular domain with Smad3. *J. Cell Biol.* **163**, 723–728 (2003).
50. Elyaman, W. *et al.* Notch receptors and Smad3 signaling cooperate in the induction of interleukin-9-producing T cells. *Immunity* **36**, 623–634 (2012).

ONLINE METHODS

Subjects. Material was collected from a total of six subjects (four male and two female). The median age of subjects was 58 years. Three patients underwent a lobectomy for a peripheral primary lung tumor, and three received lung transplantation because of end-stage pulmonary disease. Patients with a history of asthma or a recent (<4 weeks) lower respiratory tract infection at the time of inclusion in the study or in the recent past were excluded from the study. None of the patients received systemic corticosteroids, immunosuppressive therapy, chemotherapy or radiotherapy. All subjects were former smokers. Lobectomy patients were recruited from the Academic Medical Center and the Tergooi Hospitals. Two of the lobectomy patients had normal lung function and one had mild chronic obstructive pulmonary disease. All transplantation patients received a double lung transplant and were recruited from the University Medical Center Groningen. All patients gave written informed consent before inclusion in the study, and the study was approved by the Ethical Review Board (ERB) of the Academic Medical Center and the local ERBs of the other participating centers according to the Declaration of Helsinki. Unrelated buffy-coat donors were retrieved from Sanquin Blood Supply Foundation, Amsterdam, the Netherlands.

Mice. *Notch1*$^{fl/fl}$*Notch2*$^{fl/fl}$*Cd4*-Cre^{+} mice and their *Notch1*$^{fl/fl}$*Notch2*$^{fl/fl}$*Cd4*-Cre^{-} littermates, all on C57BL/6/NCrl background were bred and housed in pathogen-free conditions at the Animal Resources Center of the Academic Medical Center (AMC, Amsterdam, the Netherlands). Mice (both male and female) were between 8 and 16 weeks of age at the start of the experiment. *Notch1*$^{fl/fl}$*Notch2*$^{fl/fl}$*Cd4*-Cre^{+} mice and their *Notch1*$^{fl/fl}$*Notch2*$^{fl/fl}$*Cd4*-Cre^{-} mice were housed together to avoid 'cage bias'. Lungs of these mice were cut into small pieces and digested with Collagen type 1 (1% v/w) for 1 h at 37 °C, followed by filtration and flow cytometry. Cells were stained with the relevant fluorochrome-conjugated mAbs for 30 min at 4 °C in PBS containing 0.5% BSA and 0.02% NaN_3. For intracellular staining, cells were fixed and permeabilized using Cytofix/Cytoperm (BD Biosciences). Data acquisition and analysis was done on a LSRFortessa (Becton Dickinson) and FlowJo (Tree Star Inc.) software. To study CD103 expression on activated T cells *in vivo*, mice were intranasally infected with 100× 50% tissue culture effective dose ($TCID_{50}$) of the H3N2 influenza A virus HKx31. Viral stocks were obtained by infection of MDCK or LLC-MK2 cells[51]. At 10 d after primary infection, or 8 d after secondary infection, 1 µg anti-CD8-PE (eBioscience, clone H35-17.2) was injected intravenously 8 min before the animals were sacrificed. In this way we were able to discriminate between circulating T cells and T cells shielded from labeling within the tissues. Influenza-virus-specific CD8^{+} T cells were enumerated using a different, noncompeting antibody CD8 (BD Biosciences, anti-CD8a, clone 53-6.7, dilution 1/200) and tetramers of H-2D^{b} containing the influenza-A-virus-derived nucleocapsid protein peptide NP(366–374) (Sanquin Blood Supply Foundation). For interference of Notch signaling mice were treated with 5 mg/kg LY411575 (Sigma) in DMSO or DMSO control by intraperitoneal injection on a daily basis for up to 2 or 5 d. No weight loss or diarrhea was observed. All mice were used in accordance of institutional and national animal experimentation guidelines.

Isolation of mononuclear cells from peripheral blood and lung tissue. Heparinized peripheral blood samples were obtained before or during the surgical procedure. Peripheral blood mononuclear cells (PBMCs) were isolated using standard density gradient techniques. Directly after lobectomy, a piece of peripheral lung tissue as far from the tumor as possible was cut off by a pathologist. Lung mononuclear cells (LMCs) were isolated from this tissue specimen as described[52]. In brief, tissue specimens (1 cm × 1 cm) were sliced with a McIlwain tissue chopper into pieces of 1 mm and incubated for 20 min in RPMI with 20 mM HEPES, pH 7.4, 15% FCS (FCS) and 50 U/ml DNAse type I (Sigma-Aldrich) while shaking at 37 °C. Tissue pieces were carefully dried with sterile gauze and were transferred to medium supplemented with collagenase type I 300 U/ml (Worthington). The material was incubated in this medium for 60 min while shaking at 37 °C. A cell suspension was obtained by grinding the tissue through a flow-through chamber. Mononuclear cells were isolated from the lung cell suspension by standard density gradient techniques. To exclude the possibility of contamination with peripheral blood, the erythrocyte counts were confirmed to be less than 5% of erythrocyte counts in the paired blood sample. Isolated cells were cryopreserved in liquid nitrogen for later analysis. Due to the low frequency of CD103^{+} T cells in peripheral blood, this subset was obtained from non-related buffy coat donors. Overnight T cell stimulation was performed by adding anti-CD3 plus anti-CD28 Dynabeads (Lifetechnologies) in a 1:1 ratio (c:b) for a period of 16 h. Intracellular cytokine production was measured by stimulation of prepared lymphocyte fractions with PMA (1 ng/ml, Life Technologies) and ionomycin (1 µM, Life Technologies) for up to 6 h in the presence of brefeldin A (5 µg/ml, Life Technologies). Then cells were labeled for markers of T cell subsets as described above and fixed and permeabilized (FoxP3 buffers kit, eBioscience), and intracellular IFN-γ (anti-IFN-γ PE; BioLegend, clone 4S.B3, dilution1/400) was measured by flow cytometry. For *in vitro* stimulation with Notch ligands, CD8^{+} T cells isolated by MACS (Miltenyi Biotec) were cultured for 4 h with recombinant sDLL1 and sDLL4 (5 µg/ml, Peprotech) and RNA was isolated. For analysis, a standard Student's *t*-test (unpaired) was applied with GraphPad Prism 6 software. *P* values of <0.05 were considered statistically significant.

Analysis and cell sorting by flow cytometry. Human PBMCs or LMCs were incubated with the following antibodies: anti-CD103 PE-Cy7 (eBioscience, clone B-Ly7, dilution 1/200), anti-CD103 PE (eBioscience, clone B-Ly7, dilution 1/100), anti-CD27 FITC (Pelicluster, clone CLB-27/1, dilution 1/25), anti-CD45RA PerCP-Cy5 (eBioscience, clone HI100, dilution 1/200), anti-CD8 APC (BD, clone RPA-T8, dilution 1/100), anti-CD69 BUV395 (BD, clone FN50, dilution 1/50), anti-GZMB AF700 (BD, clone GB11, dilution 1/400), anti-PD1 (BioLegend, clone EH12.2H7, dilution 1/50), anti-anti-Tbet BV421 (BioLegend, clone 4B10, dilution 1/50), anti-EOMES eF660 (eBioscience, clone WD1928, dilution 1/400), anti-CXCR3 PE (R&D, clone 49801, dilution 1/10), anti-CCR5 PE (BD, clone 2D7, dilution 1/25), anti-CXCR6 AF647 (BioLegend, clone K041E5, 1/25) and anti-KLRG1 clone 13F12F2 (dilution 1/400, ref. 53). To prevent premature activation of T cells following staining with anti-CD3, this marker was left out of the phenotyping panel. Hence, NK cell contamination was prevented through the use of anti-CD16 PE (BD, clone 3G8, dilution 1/100) and anti-CD56 PE (BD, clone B159, dilution 1/100) as negative selection criteria. Cells used for transcriptome analysis were CD8^{+}CD45RA^{-}CD103^{+} or CD103^{-} and negative for antibodies from the NK cell mix. Near-IR and Red LIFE/DEATH fixable dyes (ThermoFisher) were used to stain death cells. Cells were labeled according to manufacturer's instructions and were washed and analyzed in PBS containing 0.5% (w/v) bovine serum albumin (BSA). Cells were analyzed or sorted with a purity >99% using a LSR Fortessa (BD Biosciences) and FACSAria III cell sorter (BD Biosciences), respectively. Analysis was performed using FlowJo software (Tree Star Inc). For analysis of mouse T_{RM} cells, the following antibodies were used: anti-CD8β AF700 (eBioscience, clone Ly-2, 53-6.7, dilution 1/200), anti-CD62L FITC (eBioscience, clone MEL-14, dilution 1/400), anti-CD44 BV785 (eBioscience, clone IM7, dilution 1/200), anti-CD69 eF450 (eBioscience, clone H1.2F3, dilution 1/200), anti-KLRG1 PECY7 (eBioscience, clone 2F1, 1/200), anti-CD103 PerCPCy5.5 (BD, clone M290, dilution 1/200), anti-CD4 Qd605 (Thermofisher, clone RM4-5, dilution 1/1000) anti-CD3 BV510 (BioLegend, clone 17A2, dilution 1/200), anti-DLL1 PE (eBioscience, clone HMD1-5, dilution 1/200), anti-Jagged1 PE (eBioscience, clone HMJ1-29, dilution 1/200), anti-Jagged2 PE (eBioscience, clone HMJ2-1, dilution 1/200), anti-Notch1 PE (BioLegend, clone HMN1-12, dilution 1/200), anti-Notch2 APC (BioLegend, clone HMN2-35, dilution 1/200). For statistical analysis of flow cytometry data, a two-way ANOVA was applied with GraphPad Prism 6 software. *P* values of <0.05 were considered statistically significant. Numerical analysis of human and mouse lung T_{RM} cells within the post-sort fractions is demonstrated in **Supplementary Table 3**.

RNA isolation, amplification, labeling and hybridization. RNA was isolated from 36 sorted cell samples (average of 83 × 10^3 cells per sample) with the Qiagen RNeasy Plus Micro kit according to manufacturer's instructions. Amplification, labeling, hybridization and data extraction were performed by ServiceXS (Leiden, the Netherlands). Hybridization was performed on the Whole Human Genome HT12-Microarrays (Illumina). The arrays were scanned using the Illumina iScan array scanner and the data retrieved using Illumina's GenomeStudio v2011.1 software. Eight microarray samples were excluded after hybridization, since their average signal was too low.

Microarray pre-processing and data-analysis. Analyses were carried out with packages from Bioconductor in the statistical software package R (version 3.0.0). Normexp-by-control background correction, quantile normalization, and $\log_2$ transformation[54] were performed on the Illumina sample and control probe profiles using the limma package (version 3.16.8). The arrayQualityMetrics package (version 3.16.0) was used to assess whether the microarray data were of good quality. Only probes detected (detection *P* value, <0.05) on at least one array were included in the differential expression analysis. Gene-wise linear models were fitted using the limma package. Differential gene expression between the different conditions was assessed via a moderated *t*-test. The resulting *P* values were corrected for multiple testing using the Benjamini-Hochberg false-discovery rate (FDR). The illuminaHumanv4.db package (version 1.18.0) was used to update the probe annotation provided by Illumina. Principal-component analysis was performed on unscaled data (function prcomp). The variance explained by the first two principal components was calculated as percentage of the total variance. Hierarchical clustering was done with Pearson correlation as distance measure and complete linkage as agglomeration method (function hclust). Gene set enrichment analysis was perfomed using CAMERA (limma package). CAMERA tests whether a set of genes is highly ranked relative to other genes in terms of differential expression, accounting for inter-gene correlation. CAMERA was applied using gene-set collections C2, C3, C5 and C7 from the Molecular Signatures Database (MSigDB v4.0) that contains information about curated, motif and gene ontology (GO) gene sets and immunological signatures. Low-quality probes that according to the updated probe annotation match repeat sequences, intergenic or intronic regions, or are unlikely to provide specific signal for any transcript were filtered out in the CAMERA analysis. In case multiple probes mapped to the same Entrez Gene ID according to the updated probe annotation, the probe with highest s.d. of its expression values was chosen. *P* values were calculated for each gene set for two alternative hypotheses (up or down). Gene-set–enrichment results were visualized using the EnrichmentMap Cytoscape plug-in. The enrichment map was generated including all gene sets with a *P* value < 0.02 and similarity cutoff value of 0.5. Singletons were removed to create the final gene-set interaction network. For network analysis, the STRING 9.1 functional protein interaction database was used[55]. Confidence view of known and predicted interactions between was applied. Edges represent functional associations; stronger associations are represented by thicker lines. Node colors indicate groups of proteins that are most related according to K-means clustering.

RNA-sequencing pre-processing and data-analysis. RNA was isolated from 200–1,500 T cells. Samples were precipitated in 0.3 M sodium acetate (Sigma), 2 µg glycogen (Thermo Scientific) and 70% ethanol overnight at –20C. After washing in 70% ethanol, RNA pellets were dissolved in primer mix and incubated for 2 min at 70 °C and processed[56]. cDNA libraries were sequenced on an Illumina HiSeq 2500 using 50-bp paired-end sequencing. For analysis of paired end CEL-seq reads, sample-specific barcodes in the 'left' reads were used for barcode splitting with the FASTX-Toolkit (version 0.0.12), and the 'right' reads were aligned to the mouse genome (UCSC, mm10) with TopHat (version 2.1.0). All reads that aligned to (exonic regions of) genes annotated by Ensembl (release 78) were quantified using featureCounts (version 1.4.3-p1). Reads were normalized using edgeR[57] (version 3.10.5) in R (version 3.2.2), and genes were removed that had less than 1 cpm in three or fewer samples. Multidimensional scaling (MDS) plots were made to detect outlier samples and two samples from one mouse were removed from further analysis. To find genes expressed differentially by $CD69^+$ DMSO-treated cells relative to their expression by $CD69^-$ DMSO-treated cells, edgeR's GLM likelihood ratio test was used, taking variation into account caused by study design. To find genes expressed differentially by $CD69^+$ GSI treated cells at day 2 relative to their expression by $CD69^-$ GSI treated cells at day 2, or by $CD69^+$ GSI treated cells at day 2 relative to their expression by $CD69^+$ DMSO treated cells at day 2, the GLM likelihood ratio test was used, taking variation caused by study design into account. FDR correction for multiple testing was used, and adjusted *P* values of <0.05 were considered significant.

Quantitative PCR. Quantitative PCR analysis was performed in duplicates with an StepOnePlus Real-Time PCR System (Applied Biosystem) using Power SYBR Green (Applied Biosystem). Reaction mixtures were incubated for 10 min at 95 °C, followed by 40 cycles of 15 s at 95 °C, 1 min at 60 °C, and, finally, 15 s at 95 °C, 1 min 60 °C and 15 s at 95 °C. Gene expression was normalized by the S18 rRNA in each sample. The primers used are listed in **Supplementary Table 4**.

Statistical analysis. All procedures were approved by the local Animal Ethics Committees. For pairwise comparisons, a standard two-sided Student's *t*-test (paired or unpaired when applicable), was applied with GraphPad Prism 6 software. *P* values of <0.05 were considered statistically significant. Gene-E v3.0.206 software, developed by the Broad Institute, was used to generate heat maps and perform hierarchical clustering. Values were converted to heat map colors using the mean and maximum values for each row. Spearman's rank correlation with average linkage was used for clustering. For statistical analysis of flow cytometry data, two-way ANOVA with the Bonferroni post-hoc test was applied with Graphpad Prsim 6 software.

51. Bodewes, R. *et al.* Vaccination against human influenza A/H3N2 virus prevents the induction of heterosubtypic immunity against lethal infection with avian influenza A/H5N1 virus. *PLoS One* **4**, e5538 (2009).
52. Holt, P.G. *et al.* Extraction of immune and inflammatory cells from human lung parenchyma: evaluation of an enzymatic digestion procedure. *Clin. Exp. Immunol.* **66**, 188–200 (1986).
53. Marcolino, I. *et al.* Frequent expression of the natural killer cell receptor KLRG1 in human cord blood T cells: correlation with replicative history. *Eur. J. Immunol.* **34**, 2672–2680 (2004).
54. Shi, W., Oshlack, A. & Smyth, G.K. Optimizing the noise versus bias trade-off for Illumina whole genome expression BeadChips. *Nucleic Acids Res.* **38**, e204 (2010).
55. Snel, B., Lehmann, G., Bork, P. & Huynen, M.A. STRING: a web-server to retrieve and display the repeatedly occurring neighbourhood of a gene. *Nucleic Acids Res.* **28**, 3442–3444 (2000).
56. Grün, D. *et al.* Single-cell messenger RNA sequencing reveals rare intestinal cell types. *Nature* **525**, 251–255 (2015).
57. Robinson, M.D., McCarthy, D.J. & Smyth, G.K. edgeR: a Bioconductor package for differential expression analysis of digital gene expression data. *Bioinformatics* **26**, 139–140 (2010).

doi:10.1038/ni.3589

Erratum: Programs for the persistence, vigilance and control of human CD8$^+$ lung-resident memory T cells

Pleun Hombrink, Christina Helbig, Ronald A Backer, Berber Piet, Anna E Oja, Regina Stark, Giso Brasser, Aldo Jongejan, René E Jonkers, Benjamin Nota, Onur Basak, Hans C Clevers, Perry D Moerland, Derk Amsen & René A W van Lier
***Nat. Immunol.* 17, 1467–1478 (2016); published online 24 October 2016; corrected after print 28 November 2016**

In the version of this article initially published, the word 'products' was misspelled (as 'prducts') in the final sentence of the third paragraph of the introduction; in Table 1, the third column was incorrectly labeled 'FDR' instead of the correct 'Genes in set'; the citation in the penultimate sentence of paragraph 1 of the third Results subsection (Chemokine and homing receptors) was incorrectly noted as a Supplementary Figure and should be cited as "(Fig. 3b)" instead; in Figure 5f, the *P* values defining the horizontal dashed lines were not visible and should be moved right for greater visibility, and each is $P = 0.05$; and in the legend to Figure 6b, 'CPM' was incorrectly defined as 'counts per minute' instead of the correct 'counts per million'. These errors have been corrected in the HTML and PDF versions of the article.